Iceberg evolution modelling: a background study

Veitch, Brian; Daley, Claude

Publisher's version / Version de l'éditeur:
https://doi.org/10.4224/12341002
PERD/CHC Report, OERC Report; no. OERC-2000-002, 2000-05-06

Iceberg Evolution Modeling
A Background Study

Prepared for
National Research Council of Canada

By

Brian Veitch and Claude Daley
Faculty of Engineering and Applied Science
Memorial University of Newfoundland

May 6, 2000

St. John's, NF, A1B 3X5
Canada

Memorial
University of Newfoundland

PERD

TABLE OF CONTENTS

SYMBOLS

a	Wave height	m
c	Specific heat capacity, cohesion	$J \cdot kg^{-1} \cdot °C^{-1}$, MPa
d	Grain size	m
g	Gravitational acceleration	$m \cdot s^{-2}$
I	Insolation	$W \cdot m^{-2}$
k	Thermal diffusivity	$m^2 \cdot s^{-1}$
t	time	s, days
K	Thermal conductivity	$W \cdot m^{-1} \cdot °C^{-1}$
L_f	Specific latent heat of fusion	$J \cdot kg^{-1}$
L_v	Specific latent heat of vaporization	$J \cdot kg^{-1}$
L_{WL}	Waterline length of iceberg	m
T	Temperature	°C
M	Mass of the iceberg	kg
N_u	Nusselt number	-
P_r	Prandtl number	-
q_w	Heat transfer per unit area	$W \cdot m^{-2}$
R	melt rate	$m\ day^{-1}$
Re	Reynolds number	-
S	Surface area, strength	m^2, MPa
V	Volume	m^3
$\boldsymbol{V}_i$	Horizontal drift velocity	$m \cdot s^{-1}$
$\boldsymbol{F}_B$	Buoyancy force	N
$\boldsymbol{F}_C$	Coriolis force	N
$\boldsymbol{F}_{Da}$	Air drag force	N
$\boldsymbol{F}_{Dw}$	Water drag force	N
$\boldsymbol{F}_{Di}$	Sea ice indentation force	N
$\boldsymbol{F}_{Wr}$	Wave radiation force	N
$\boldsymbol{F}_W$	Weight force	N
$\boldsymbol{F}_P$	Horizontal pressure gradient force	N
α	Albedo	-
$\dot{\varepsilon}$	Strain rate	s^{-1}
σ	Ice strength, stress	$N \cdot m^{-2}$
τ	Ice shear strength,	$N \cdot m^{-2}$
ρ_i	Density of ice	$kg \cdot m^{-3}$
ρ_{io}	Density of pure ice	$kg \cdot m^{-3}$
ρ_w	Density of water	$kg \cdot m^{-3}$

ACKNOWLEDGEMENT

The work was made possible with the support of funding from PERD (Panel on Energy Research and Development). The authors wish to thank Dr. Robert Frederking of the NRC/CHC (Canadian Hydraulics Centre) for his support and patience.

1 Introduction

The presence of icebergs poses unique risks to shipping and oil and gas industry operations and subsequently to the ocean environment. These include risks of impact on fixed and floating installations, risks of collision with conventional ship navigation, and risks of scour on sub-sea installations, such as pipelines and wellheads. The consequences of iceberg impact can be severe in terms of the structural integrity of installations, and the safety of personnel and the environment. This is of immediate concern to the current activities offshore Newfoundland.

In assessing iceberg risks, there are several critical components. The population of icebergs is the most important piece of data. Iceberg mass is of similar importance. These two issues have received the most attention to date. However in order to assess specific risks it is necessary to have more data. Shape, movement, and stability are important parameters in modeling the risks due to a collision. Finally, the ice mechanical strength and contact pressures determine the actual interaction effects.

The present work is aimed towards the eventual development of a detailed model of iceberg evolution. While the shape, movement and stability issues are primarily being addressed, iceberg evolution modeling is important to the population, mass and mechanical property issues as well. Icebergs in the Newfoundland and Labrador offshore environment change rapidly as they migrate from northern latitudes where they originate, to the latitudes around Newfoundland where they disappear. The changes are due to wave erosion and associated calving, natural and forced convective melting, solar radiation melting, and fragmentation due to thermal and motion induced stresses, and reorientation.

The approach taken here is to outline a preliminary model based on a thorough review of the existing state of knowledge of iceberg evolution in terms of thermodynamic decay and fragmentation. In doing so, the most important physical processes are recognized. Weaknesses in the state of knowledge are identified and an approach for addressing these issues in future is presented. The ultimate aim of the work is to develop a model of the iceberg evolution process that can be used as an experimental tool to improve understanding and to find in these processes the dominant characteristics that can inform iceberg risk assessment. Necessarily, the development and validation of this model requires empirical calibration and separate validation.

2 Description of Icebergs

2.1 Formation of glacial and iceberg ice

Glacial ice is formed from snow. The transition from snow to ice is gradual and depends on temperature and pressure. Warmer temperatures, such as those experienced at temperate glaciers, speed the transition. The process is slower on the colder Polar glaciers. The transition from snow to ice occurs when air pockets within and between grains no longer connect, which occurs at a density of about 830 $kg \cdot m^{-3}$. As the density of pure ice is about 917 $kg \cdot m^{-3}$, air bubbles can make up to about 10% of the volume of ice. Further increases in glacial ice density from about 830 $kg \cdot m^{-3}$ requires that the air bubbles, which are typically on the order of a tenth of a millimeter in diameter, be compressed. Depths at which the ice transition has been measured are variable, but 50m to 90m are typical. Densities for types of snow and ice are given in Table 1. Glacial ice crystals tend to be randomly oriented and are typically 1 to 4 mm across, although they can be considerably larger. Paterson (1994, pp.8-25) gives a more comprehensive description of glacial snow and ice.

Table 1. Densities of snow and ice (after Paterson, p.9).

Description	ρ
	$[kg \cdot m^{-3}]$
New snow - settled snow	50-300
Depth hoar and wind packed snow	100-400
Firn and wet snow	400-830
Glacier ice	830-917

Reported values of porosity from five icebergs grounded along the coast of Newfoundland yield an average density of approximately 893±7 $kg \cdot m^{-3}$ (Gammon *et al*. 1983). The same measurement program indicated that the iceberg ice contained few impurities and had a mean grain size of about 15mm. Mean crack densities of 0.35/cm and 0.26/cm for two of the icebergs were reported, where crack density is defined as the number of visible cracks per unit length along a straight line. Sources of cracks include glacial origins, thermal stress induced cracks, and cracks from stress due to hydrostatic and dynamic forces.

The authors also reported results of a set of 11 uniaxial compression tests of iceberg ice done at an average of -4.2°C over a narrow range of temperature and an approximately constant strain rate of $1.085 \times 10^{-3} s^{-1}$. The mean values of the elastic modulus and uniaxial compressive strength were 6092 MPa and 5.34 MPa, respectively. They did tests with freshwater ice for comparison

and found that iceberg ice was about 35% stronger and tended to be less brittle, which the authors speculated could be due to possible stress diffusing effects of bubbles near crack tips, which may inhibit crack propagation in iceberg ice.

Subsequent laboratory triaxial, uniaxial, and flexural strength experiments that were done over a range of temperatures and strain rates with ice from four icebergs and a glacier indicated that bubbles may have an important effect on uniaxial and flexural strength (Gagnon & Gammon 1995a, 1995b). This laboratory work included detailed measurements of bubbles, crystal structure, and crack density (a mean of 0.63/cm was measured). Reported values of fractional porosity indicated density values in the range between 886 $kg \cdot m^{-3}$ and 910 $kg \cdot m^{-3}$, with a mean of 895 $kg \cdot m^{-3}$, which is similar to the earlier findings.

There were considerable variations in the results from different ice sources, but some representative results can be shown here to give an indication of the mechanical properties of iceberg ice. For example, results of 24 flexural strength tests done at a strain rate of $10^{-3}s^{-1}$ between -1°C and -16°C indicated that the flexural strength S_f depended on temperature according to

$$S_f = 0.8827 - 0.0738T - 0.00213T^2 \quad (1)$$

so that, for example, the flexural strength at -10°C is 1.41 MPa.

A summary of the results of some of the triaxial tests reported by Gagnon & Gammon 1995b is presented in Table 2. Note that the each of the 20 data sets referred to in column 1 consisted of 5 experiments.

Other laboratory experiments on iceberg ice have been reported by El-Tahan *et al*. (1984). They did uniaxial, multiaxial, and indentation tests with small test samples at moderately high strain rates meant to reflect their interest in iceberg impact loads.

Another physical characteristic of glacial ice and icebergs is the presence of large cracks and other defects, such as firn covered crevasses, which can extend for several kilometers in length and be several tens of meters deep (Bader 1977, Kovacs 1977). Crevasses can fill with snow and frost and can eventually transform into ice, or approach the transformation point, but remain weak in tensile strength compared to surrounding ice. In glaciers and tabular icebergs, these flaws tend to be vertical, but not parallel.

Table 2. Triaxial compressive strength (after Gagnon & Gammon 1995b).

data set	mean strength S	standard deviation	confining pressure	strain rate $\dot{\varepsilon}$	temperature T
	[MPa]	[MPa]	[MPa]	[10^{-3} s^{-1}]	[C]
1	4.43	1.00	0.00	1.45	-1
2	10.29	0.68	1.38	3.93	-1
3	10.17	0.95	3.45	4.34	-1
4	10.74	1.07	6.89	4.84	-1
5	8.67	0.60	13.79	5.13	-1
6	12.27	0.95	1.38	3.76	-6
7	13.22	0.85	6.89	4.73	-6
8	7.82	1.63	0.00	1.63	-11
9	10.75	0.84	1.38	77.50	-11
10	14.64	0.89	1.38	3.46	-11
11	3.50	0.21	1.38	0.0482	-11
12	11.98	1.21	3.45	75.50	-11
13	13.19	1.83	3.45	4.17	-11
14	13.79	1.83	6.89	58.50	-11
15	16.05	0.78	6.89	4.21	-11
16	4.75	0.35	6.89	0.0596	-11
17	14.97	1.34	13.79	32.00	-11
18	16.01	0.61	13.79	5.67	-11
19	18.42	1.26	1.38	3.99	-16
20	19.71	2.33	6.89	5.57	-16

2.1.1 Thermodynamic parameters

As thermodynamic processes are important in iceberg evolution, values of some basic parameters drawn from the literature are presented below.

Table 3. Thermal parameters of pure ice at 0°C.

Specific latent heat of fusion[1]	L_f	3.335×10^{5}	$J\cdot kg^{-1}$
Specific latent heat of vaporization[2]	L_v	2.832×10^{6}	$J\cdot kg^{-1}$
Specific heat capacity[2]	c	2.115×10^{3}	$J\cdot kg^{-1}\cdot°C^{-1}$
Thermal conductivity[2]	K	2.238	$W\cdot m^{-1}\cdot°C^{-1}$
Thermal diffusivity	k	1.15×10^{-6}	$m^{2}\cdot s^{-1}$

[1] Paterson 1994, p.205.
[2] Pounder 1965, p.117-118.

Paterson (1994, p.205) relates specific heat capacity and thermal conductivity to temperature T according to

$$c = 2097 + 7.122T \tag{2}$$

$$K = 2.073e^{-5.7\times10^{-3}T} . \tag{3}$$

Thermal conductivity is also dependent on ice density. Pounder (1965, p.117) gives a somewhat different formulation for c and K.

$$c = 2115 + 7.793T \tag{4}$$

$$K(T) = 2.238\left(1 - 4.8\times10^{-3}T\right) \tag{5}$$

$$K(\rho_i) = \frac{2K\rho_i}{3\rho_{io} - \rho_i} \tag{6}$$

where ρ_{io} is the density of pure ice. Pounder's values for K(0°C) are similar to Hobbes' (1974, p.361) and are used here, as is his expression for c. Thermal diffusivity can be found from

$$k = \frac{K}{\rho_i c} \tag{7}$$

Albedo, the ratio of reflected to incident energy, is an important parameter for insolation. Values are presented in Table 4 for a variety of ice and snow surfaces.

Table 4. Albedo of snow and ice surfaces (after Paterson, p.59).

Ice surface	Albedo range	Mean albedo
	α [%]	α [%]
Dry snow	80-97	84
Melting snow	66-88	74
Firn	43-69	53
Clean ice	34-51	40
Slightly dirty ice	26-33	29
Dirty ice	15-25	21
Debris-covered ice	10-15	12

The freezing temperature of 3.5% salinity sea water is about -1.8°C. Water density is dependent on salinity and temperature: for sea water between -1.8°C and 10°C the density ranges from 1028 $kg \cdot m^{-3}$ and 1027 $kg \cdot m^{-3}$.

2.1.2 Iceberg calving

Glaciers are the source of all icebergs. In fact, iceberg calving is by far the most important component of glacial ablation. The other components are surface melting and run-off, surface sublimation and evaporation, and underside surface melting of floating ice shelves. Not all glaciers are iceberg calving sites; only those with ocean termini can produce icebergs. Termini can be either floating or grounded. Temperate tidewater glaciers are grounded at their termini, often in shallow water or on a glacial moraine shoal. The iceberg calving rates at these types of glaciers can be highly unsteady.

A study of fifteen temperate glaciers in southern Alaska, for example, indicated that the glaciers were relatively stable while the termini were grounded on shoals, but when a terminus retreated off the shoal and into deeper water, the calving rates increased and the terminus retreated dramatically. This led to a hypothesis that calving rate was a simple function of water depth at the terminus and independent of climatic conditions (Brown *et al.* 1982). Significantly, this intensive study was done in response to an expectation that the Columbia Glacier was about to undergo a drastic increase in calving rate, which would have the consequence of increasing the risk of iceberg collision with oil tanker traffic in the nearby shipping lanes to the port of Valdez. This turned out be prescient when, within several years, the Columbia Glacier retreated rapidly (Krimmel and Vaughn 1987).

Brown *et al.*'s empirical calving rate relationship for temperate grounded tidewater glaciers, and similar simple relationships (e.g. Sikonia 1982), have been used in models to predict glacier

dynamics (e.g. Bindschadler & Rasmussen 1983), but these are concerned primarily with gross mass balance predictions and do not provide any insight to the size and shape of the icebergs calved. Further, the relationships do not apply to glaciers with floating termini, although this has been addressed by Pelto and Warren (1991) in their study of the calving rates of 22 Polar and temperate glaciers with grounded and floating termini.

According to Paterson (1994) and Meier and Post (1987), net mass balance models of glaciers do not yet provide reliable estimates, which is due in part to the difficulty of predicting calving and basal melting ablation terms for both grounded and floating termini. Neither the empirical relationships mentioned above, nor mechanics based attempts to model calving (e.g. Reeh 1968, Holdsworth 1973, 1977) appears to have won much confidence.

Some insight into the size and shape of icebergs at calving sites has been offered by Dowdeswell *et al*. (1992) based on a field observation program of the Scoresby Sund Fjord glaciers in East Greenland. They found that fast moving outlet glaciers with floating or partially floating termini produce the bulk of icebergs in terms of gross mass and that icebergs calved at these types of glaciers include large and very large tabular icebergs. This echoes Robe's (1980) conclusion that floating termini produce tabular icebergs whose length and width are a function of the unsupported part of the glacier, and that ice shelves can produce the biggest tabular icebergs. Tidewater glaciers grounded in relatively shallow water produce smaller and more irregularly shaped icebergs. Iceberg production at this type of site comprises a smaller proportion of the total mass of calved ice than from the fast outlet glaciers. As they are grounded, the maximum dimension of the icebergs that can calve is the vertical extent of the termini.

Dowdeswell *et al*. (1992) also noted that local bathymetry has an important influence on the fate of icebergs. Specifically, large icebergs can be effectively trapped inside coastal regions due to water depth restrictions. One of the interesting features of the iceberg size distribution data they collected was that the proportion of smaller icebergs decreased with distance from the source, which they attributed to the deterioration of smaller irregularly shaped icebergs. This implies that larger icebergs, which means large tabular icebergs, have a higher likelihood of surviving long enough to drift as far as south the Labrador Sea or Grand Banks. A set of initial conditions for an iceberg shape evolution model could reasonably include a tabular shape.

Icebergs that eventually drift south to the Labrador Sea and onto the Grand Banks originate primarily at calving sites in West Greenland. The ice shelves of northern Ellesmere Island (Ward Hunt, Mclintock, Ayles, to name three), which produce floating ice islands, are a minor source. Most East Greenland icebergs are prevented by either bathymetry or landfast sea ice from drifting far from their sources. A few East Greenland icebergs drift south in the East Greenland Current and are picked up by the West Greenland Current and carried north into Baffin Bay or

south in the Labrador current. Exposure to waves and warm water during such a drift pattern would be expected to cause considerable deterioration.

The Polar and sub Polar West Greenland glaciers frequently have floating termini. There is usually no snow cover nor firn at the termini of Greenland glaciers (Robe 1980), so the ice density is relatively uniform, unlike Antarctic icebergs. The largest iceberg producing site in West Greenland is the Jakobshavn Isbræ (approximately 69ºN), whose production of icebergs has been estimated at between 2×10^{13} and 4×10^{13} kg per year and whose terminus has been observed to move up to 23 meters per day - the fastest tidewater glacier. Most of the calf ice sites south of Jakobshavn in West Greenland produce less than 2×10^{12} kg per year (Weidick *et al.* 1992). Some other important calving sites north of Jakobshavn are Rinks (71°45'N), Upernavik, Hays (74°50'N), and Kjaers Glaciers and Steenstrup ice sheet, Gades, Tracy, and Heilprin Glaciers, and the massive northern Humbolt and Petermanns Glaciers (Kollmeyer 1980). All together, about 10^{14} kg of ice calves each year from the West and North Greenland glaciers, with an average iceberg size of about 5×10^{9} kg (Robe 1980).

The floating termini of Greenland glaciers are typically between 200 m and 300 m thick, although there is considerable variation. For example, Rinks Glacier calves icebergs 600 m thick, although the local bathymetry can delay the seaward movement of such icebergs (Robe 1980).

2.1.3 Iceberg statistics

The West Greenland icebergs typically drift across Baffin Bay and then south along Baffin Island and into the Labrador Sea off the coast of Labrador (e.g. Robe *et al.* 1980). Of the estimated 10,000 icebergs calved annually, many never make it far from their calving sites, and others become grounded along the coasts of either Baffin Island or Labrador. While most of these icebergs are tabular at their sources (e.g. Holdsworth 1977) and routinely reach 1 km in length, by the time they reach the Grand Banks after an average of approximately 3 years, they are irregularly shaped remnants of the originals, having typically diminished to 1×10^{6} to 3×10^{6} tonnes (Kollmeyer 1977).

While drifting in the Arctic, icebergs can be locked into land fast and pack ice for substantial periods of the year. When the sea ice breaks up, the icebergs can move more freely and it is during the break up and brief summer open water season that icebergs can drift out of the Arctic and into the open ocean via the Labrador Current.

As they drift past Labrador, (average drift speed is 0.25 to 0.5 m/s (Robe 1980)) icebergs occasionally drift through the Strait of Belle Isle and into the Gulf of St. Lawrence, although the

vast majority continue on a roughly south-easterly heading. Many of these become grounded and deteriorate in Notre Dame Bay, Bonivasta Bay, and other northerly facing bays along the north coast of Newfoundland. Others parade south along the east coast of the Avalon Peninsula. Of the remaining icebergs, most take a circuitous route that follows the bathymetry over the Grand Banks through the Flemish Pass. The impressive compilation of iceberg sightings from the historical record between 1810 and 1958 that Hill (1999) presented and which is reproduced in Figure 1 illustrates this nicely. Only very rarely do icebergs drift south of 40°N or east of 40°W (Ketchen & Hildenbrand 1977).

There have been a few studies of iceberg populations over the years, one of the earliest being by Gustajtis & Buckley (1977) who used IIP flight data to look at the seasonal variability of iceberg population on the Labrador Coast. Morgan and Budd (1977) tried to infer melt rates from iceberg population statistics for Antarctic icebergs.

Marko (1996) analyzed several existing data sets on iceberg size distributions from areas on the Grand Banks, Baffin Bay and Labrador Sea (Norcor 1980, Petro-Canada 1982, and others) to look for physical insight into iceberg deterioration via the evolution of iceberg population statistics, with particular focus on the source of small iceberg fragments offshore Newfoundland. He found that "large" icebergs, which he defined as those with lengths greater than 20m, follow log-normal and gamma distributions well. The distributions worked well for samples from different locations and seasons. These data cover an order of magnitude of size data (from 10s to 100s of meters). For smaller icebergs (lengths less than 20m), fewer data exist (Fenco 1987, Crocker 1993, Crocker & Cammaert 1994), but what he has found indicates that occurrence probability increases exponentially with decreasing size for these smaller icebergs. Marko's interpretation of the data is interesting: he postulates that large scale fracturing, such as due to wave induced bending stresses, is the only deterioration process consistent with the observed long term maintenance of log-normal iceberg population distributions. He noted that the log-normal distribution is commonly found to describe size distributions of natural fragmentation processes.

While this is so, the piece size statistics cover only an order of magnitude and may not warrant such a strong claim yet. Interpretation of physical processes based on piece size distributions of fragmentation processes is difficult (e.g. Grady & Kipp 1989). What we have in icebergs is a population undergoing multiple and repeated breakup coupled with ablation by melting. An analogy can be drawn to meteorites, which are also fragments from a repeating break up process, that ablate as they fall through the atmosphere. These too have a characteristic piece size distribution. What Marko has pointed out, correctly in the authors' opinion, is that

there is some large scale fracture process (or processes) that is not adequately represented in existing deterioration models.

Singh *et al*. (1998) have compiled a database of over 127,000 iceberg sightings on the Grand Banks from between 1960 and 1998. The vast majority of the data is derived from International Ice Patrol (IIP) digital reports, with the remaining data coming from oil industry and other sources. The data base includes basic information about the icebergs, such as location, shape classification, and size classification. Of the 127,000 total, there are 358 recordings of iceberg mass and 436 of length, in addition to a small subset of data with length and breadth records. Also, there are a limited number of repeated sightings recorded of the same iceberg. This huge database reflects the current state of knowledge as far as iceberg sightings statistics is concerned. However, as most of the data is from the IIP, a detailed understanding of their data collection methods is essential to a proper analysis (see Anderson 1993).

Another recently compiled data base focuses on more precisely defined field measurements of iceberg dimensions and shape (Anon. 1999). This is discussed in the section of iceberg shape, below. Both databases (Singh *et al*. 1998 and Anon. 1999) were compiled under the sponsorship of the Program for Energy Research and Development (PERD) and are comprehensive enough to make it unnecessary here to either repeat the compilation process of reviewing individual papers, or extend the data base by looking for information that may have been overlooked.

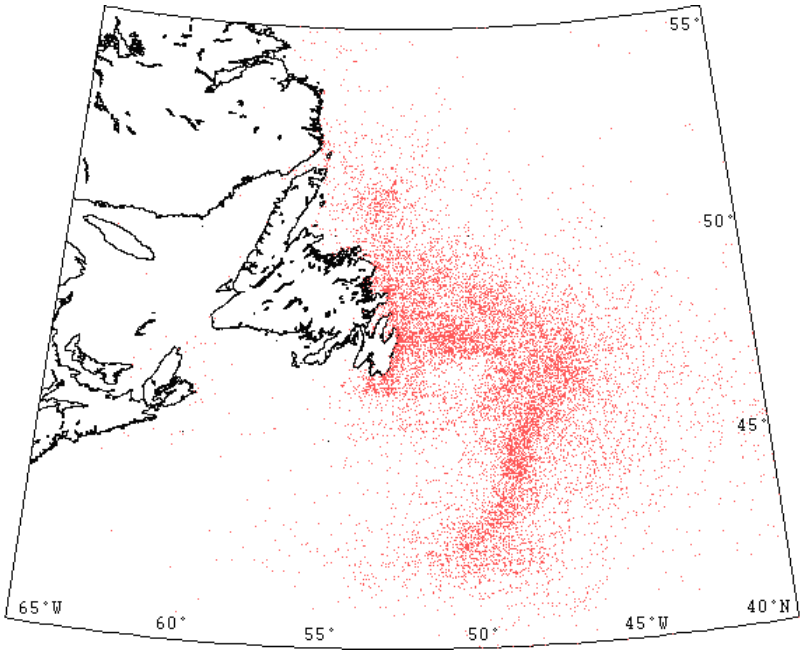

Figure 1. Distribution of about 14,000 icebergs sighted around Newfoundland between 1810 and 1958. (*Courtesy of Brian Hill*)

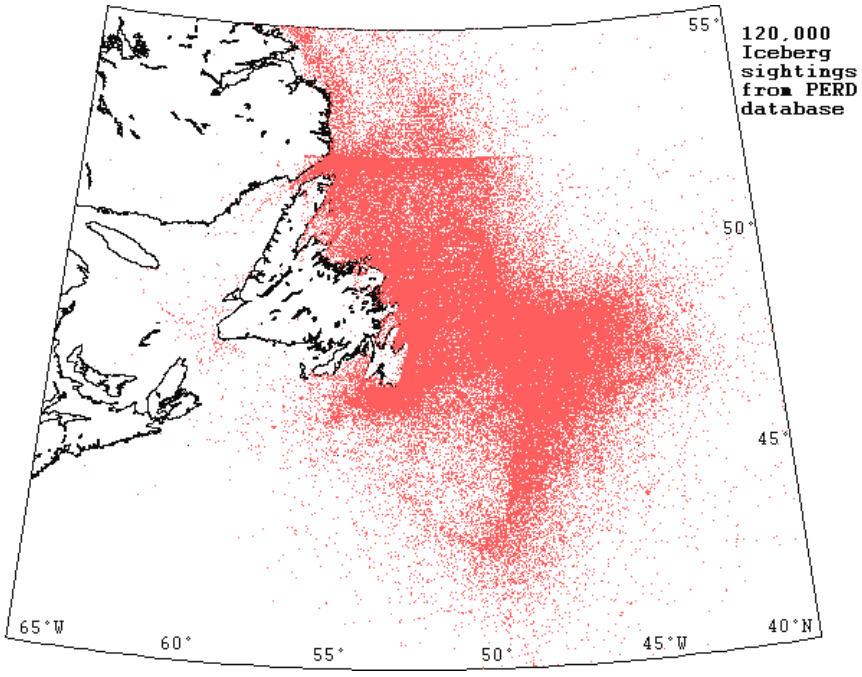

Figure 2. Distribution of about 120,000 icebergs sighted around Newfoundland between 1960 and 1998. (*Courtesy of Brian Hill*)

2.2 Iceberg drift

Iceberg drift has been of particular interest to the shipping industry for many years. The International Ice Patrol, for example, has been making observations of icebergs on the Grand Banks of Newfoundland for decades in order to provide information concerning ice and iceberg hazards to shipping. More recently, iceberg drift has become of major interest to the offshore petroleum industry, which is concerned with icebergs colliding with fixed petroleum installations (e.g. Fuglem *et al*. 1996, Isaacson & McTaggart 1990).

The IIP currently uses a drift model by Mountain (1980), along with an iceberg deterioration model by Anderson (1983, see below). Mountain's (1980) drift model was intended to be an operational model that effectively helped to span the iceberg observation intervals, which could be on the order of several days. The petroleum industry is more interested in the shorter term drift of icebergs that are in the vicinity of installations that might be at risk. Short term in this context means less than a day, which is a practical time frame for iceberg management tactics.

In terms of iceberg evolution, drift and drift predictions are not of primary interest as we are more concerned here with the physical changes in shape, rather than in position. However, it is recognized that the environmental conditions that drive the drift motion are also important for

shape evolution and for this reason it is worthwhile to take a quick look at iceberg drift and its prediction.

Some early observations and measurements of drifting icebergs (e.g. Soulis 1975, Russell *et al*. 1977, Riggs *et al*. 1980, and Robe *et al*. 1980) were made in support of the development of practical forecasting tools. Currents were found to be the most important driving force for drift. Deep steady currents were found to be relatively important for large icebergs and wind driven currents were relatively important for smaller bergs. Observations indicated that wind force was important only when the winds were quite strong (greater than 15 knots) and persistent. Added mass effects were noted as being small, but important, and the importance of the flow regime on drag and drag coefficient was emphasized (Russell *et al*. 1977). Soulis (1975) recognized in the drift patterns he measured an underlying complexity that he correctly foresaw being difficult to model.

Mountain's (1980) model is notable because it is an early model and it is still the basis of the IIP drift model. It consists of a force balance between water drag, air drag, a Coriolis term, and a sea surface slope term. The water drag term is summed up over several layers using a constant geostrophic current and a time dependent Ekman current averaged over each layer. The drag coefficients used for both air and water are 1.5. Mountain compared field data of tracked icebergs with predictions, which showed that predicted drift paths had significant random errors. He concluded that the main limitation was attributable to the accuracy of oceanographic data, particularly wind and current, that are used to drive the model, rather than the limitations in the physics based model itself. Sodhi & El-Tahan (1980) followed along much the same lines as Mountain, although they incorporated added mass effects, which they showed to be small. Neither model included wave drift force, although a drift term appears in El-Tahan *et al*. (1983).

Predictions of deterministic models all suffer the effects of the randomness in the environmental driving forces. Some investigators have tried to treat the short term drift statistically in some manner (e.g. Smith & Banke 1981, 1983, Shirasawa *et al*. 1984, Gaskill & Rochester 1984, Garrett 1985, Smith 1993), but none of these appear to be especially successful in forecasting.

More recent models (e.g. Bigg *et al*. 1996, 1997, Løset 1993, Johannessen *et al*. 1999) have also included wave radiation and sea ice forces, in addition to Coriolis, wind drag, water drag, and surface slope terms. Of these, at least Bigg *et al*. (1997) is a longer term drift model that attempts to capture large scale oceanographic phenomena and incorporates large scale oceanographic driving force information. Iceberg deterioration models incorporated in these more recent models still rely on previous work (e.g. White *et al*. 1980). The basic drift equation can be written as

$$M\frac{d\boldsymbol{V}_i}{dt} = \boldsymbol{F}_C + \boldsymbol{F}_{Da} + \boldsymbol{F}_{Dw} + \boldsymbol{F}_{Di} + \boldsymbol{F}_{Wr} + +\boldsymbol{F}_P \tag{8}$$

where M is the mass of the iceberg, $\boldsymbol{V}_i$ is the horizontal drift velocity, $\boldsymbol{F}_C$ is the Coriolis force, $\boldsymbol{F}_{Da}$ is the air drag on the above water portion of the iceberg, $\boldsymbol{F}_{Dw}$ is the water drag on the underwater portion of the iceberg, $\boldsymbol{F}_{Di}$ is the force associated with indentation of an ice sheet, $\boldsymbol{F}_{Wr}$ is the wave radiation force, and $\boldsymbol{F}_P$ is the horizontal pressure gradient force.

3 Iceberg Evolution

3.1 Ablation Processes

Iceberg ablation processes can be categorized as discrete or continuous. Thermodynamic processes are continuous and fragmentation processes are discrete. All are dependent on environmental conditions, such as wave spectra, water and air temperatures, current velocities, and winds.

Above water heat transfer and melting are due to insolation, or solar radiation, and forced convection is due to wind. As the above water volume of a typical iceberg constitutes only about 13% of the total volume, above water ablation due to thermodynamic processes tends to be relatively minor.

Underwater melting is due to natural convection associated with the buoyant vertical plume of iceberg melt water, and forced convection due to the relative motion of the iceberg and surrounding fluid. Both are dependent on water temperature.

Gravity waves incident on an iceberg lead to accelerated melting near the free water surface due to the effects of increased water particle velocities and turbulence. On a vertical ice wall, the wave erosion process causes a groove, or notch, to form along the waterline, as a result of which the above water ice wall is unsupported and overhangs the notch. Underwater, a shelf forms. For a non vertical ice wall, incident wave energy is less likely to be reflected so that wave erosion can be expected to increase. As wave erosion is dependent on wave energy, in addition to water temperature, it is sensitive to wave direction. When wave energy is focused, say due to local geometry or a local defect, wave erosion is concentrated and accelerated. This process can reinforce itself with dramatic results.

An important consequence of the notching effects of wave erosion is that the overhanging ice calves. While the volume of ice calved off at any given fragmentation event is effectively limited by the notch depth and overhang geometry, the cumulative effects of this repeating ablation mechanism are important in terms of both shape evolution and total ablation.

Other fragmentation processes are due to thermal induced stresses and to hydrostatic and inertial forces. Inertial forces associated with iceberg motion are likely to be inconsequential for large icebergs. Motion induced stresses are important during instability events that result in reorientation of the iceberg through rolling, during which global failure can occur. Likewise, weight and buoyancy force distributions can give rise to stresses that can split an iceberg in half. Similarly, bending moments due to the passage of waves can also cause splitting, but this is

likely only for very large or irregularly shaped icebergs. Large discontinuities, or defects, in the ice, such as drainage channels and crevasse defects, may play an important role in initiating large scale fragmentation events.

The photograph of an iceberg shown in Figure 3 illustrates some of the ablation process results. One of the most striking features of this particular iceberg is its varied geometry: it is evolving toward a tabular dry dock type on one side and has two pronounced pinnacles on the other. Most of the visible surfaces are quite rough and do not indicate signs of extensive melting, although broken rubble at the bases of the pinnacles may be indicative of local thermal or weight induced fragmentation. Nearer the waterline, the shape is characterized by smooth terraces at different, roughly parallel levels around its perimeter. The notch in each terrace is formed due to wave erosion. That these have emerged in what appears to have been several consecutive steps indicates that the iceberg has lost substantial amounts of ice in discrete packets. Further, the emergence of the iceberg shows that the above water ablation is dominating the underwater processes, relative to the volumes above and below water. Otherwise, the iceberg would be sinking. Calving from floating tabular icebergs has been observed to increase the freeboard to thickness ratio (Kovacs 1977) similarly. Another plausible explanation for the emergence is that the iceberg, which was grounded, was pushed into progressively shallower water.

Figure 3. Iceberg 1 in Conception Bay, 1991, looking North.

3.2 Thermodynamic processes

3.2.1 Solar radiation

Insolation I is the direct solar radiation on a horizontal surface per unit area per unit time. Insolation on an iceberg depends on latitude and local meteorological conditions, such as fog and cloud cover. Assuming that the heat transfer due to insolation goes directly to melting, then the melt rate at a horizontal surface can be calculated as;

$$\frac{d}{dt}\left(\mathbf{r}\cdot\hat{\mathbf{n}}\right)=\frac{(1-\alpha)I}{\rho_i L_f} \quad (9)$$

where $\mathbf{r}$ defines the position at which the melting occurs and $\hat{\mathbf{n}}$ is a unit normal at that point. The coordinate system here is inertial with z_o pointing down. If the surface is not horizontal, then the insolation reduces to $I\cdot\hat{\mathbf{n}}$. For example, a typical value for insolation on the Grand banks is about 300 $J\cdot m^{-2}\cdot s^{-1}$, which would result in a melt rate of about 2 $mm\cdot hr^{-1}$ for a horizontal surface and less for an inclined surface.

3.2.2 Forced convection (wind and water)

Melting due to forced convection (wind) is negligible. Melting due to forced convection (underwater melting) is largely dependent on the relative velocity and temperature of the water and ice and so is linked to currents, winds, drift, and temperatures. Theoretical treatment of this problem, or even a simplification of it (e.g. Griffin 1977), is difficult. White *et al*. (1980) gave an approximate means of evaluating the melt rates of tabular and non tabular icebergs separately:

$$\frac{d}{dt}\left(\mathbf{r}\cdot\hat{\mathbf{n}}\right)=\frac{q_w}{\rho_i L_f}=\frac{N_u K\Delta T}{\rho_i L_f L_{WL}} \quad (10)$$

where L_f is the specific latent heat of fusion of ice, ρ_i is the density of ice, ΔT is the temperature difference between the water and ice, K is the thermal conductivity of ice, and L_{WL} is the maximum waterline length of the iceberg. N_u is the Nusselt number, which in terms of Reynolds and Prandtl numbers is given as;

$$N_u = 0.055 R_e^{0.8} P_r^{0.4} \quad \text{non tabular}$$
$$N_u = 0.058 R_e^{0.8} P_r^{0.4} \quad \text{tabular} \tag{11}$$

Løset (1993b) developed a numerical model of the temperature distribution in an iceberg, which showed that the inner core temperature is remarkably stable. Some useful measurements of the temperatures at the ice-water interface have been reported by Clifford *et al*. (1980) and Fuhs *et al*. (1980) for a small block of towed ice.

3.2.3 Buoyant convection

A pair of laboratory experiments on natural buoyant convective melting and wave erosion were reported Josberger (1977) and Martin *et al*. (1977). Field work was done to validate the lab work. The first experiment looked at the natural convective boundary layer between a vertical ice wall in saltwater and the melting that occurs at the ice surface. Buoyant upwelling is driven by melt from the ice, which is colder and less saline than the ambient seawater. Diffusion of salinity and temperature occurs and the two liquids mix in what is not a simple process to model mathematically. Importantly, the buoyant plume, or boundary layer starts as laminar at the bottom of the ice wall, but changes to turbulent flow quickly (within about 0.5 m for an iceberg). There is a transition flow regime in between. Melt rate was found to be dependent on flow regime, with the transition zone having the highest melt rate (due to a horizontal jet). Melt rate was about 30% higher in the turbulent zone than in the laminar zone. The melt rate in the turbulent zone was found to be weakly dependent on position (from the transition zone). Melt rates were constant and depended on far field temperature.

The lab experiment results were tested in a field measurement program in which temperature and salinity measurements of water near an iceberg were made. The measurement program was not elaborate, nor conclusive in its detail regarding the boundary layer, but it did provide evidence that upwelling does occur. The author estimated the associated melt rate to be on the order of 0.1m/day and the boundary layer to be about 0.5m. Interestingly, the iceberg they studied in the field had recently rolled, revealing a previous waterline notch and the relatively rough above water surface features and smooth below water features, which the author interpreted as clear evidence that even in relatively cold water (about 4°C in far field) an iceberg melts faster below water than above water.

Russell-Head (1980) reported laboratory experiments in which the melting rates of ice blocks in quiescent water were measured as a function of water temperature, salinity, and ice block size. He found that basal and side melting rates were similar, but side melting was weakly dependent

on the size of the iceberg due to the insulating protection of the thicker buoyant plumes associated with bigger vertical walls. Basal melting did not appear to depend on block size. Salinity was found to be important because of its role in the formation of a buoyant plume, otherwise, it did not have a significant effect on melting. Melting rate R was found to be proportional to the difference between far field water temperature T_s and freezing temperature T_f raised to the 1.5;

$$R = 1.8 \times 10^{-2} \left(T_s - T_f \right)^{1.5} \text{ m·day}^{-1} \tag{12}$$

This result is similar in form to Josberger's scaled prediction, but the latter had a constant more than twice the former:

$$R = 3.7 \times 10^{-2} \left(T_s - T_f \right)^{1.5} \text{ m·day}^{-1} \tag{13}$$

White *et al*. (1980) have reviewed other predictions of buoyant melting.

The simple melting tests described in Annex A can be used to examine Eq.12. Using Eq.12 to describe the rate at which the melting surfaces move, and using the same assumptions as in (A12) (case 4 in Annex A), the mass versus time can be plotted. (see Figure 4). To get a good fit, either the constant or the exponent on temperature difference can be adjusted. As all the data was collected at one temperature, there is no way to determine whether a new constant or exponent is correct. The following equations produce a good fit with the data (see Figure 4);

$$R = 1.8 \times 10^{-2} \left(T_s - T_f \right)^{1.65} \tag{14a}$$

$$R = 2.7 \times 10^{-2} \left(T_s - T_f \right)^{1.5} \tag{14b}$$

There are almost certainly aspects of the melting process that are size dependent. Nevertheless, the above empirical equation is a good starting point for prediction of melting of icebergs.

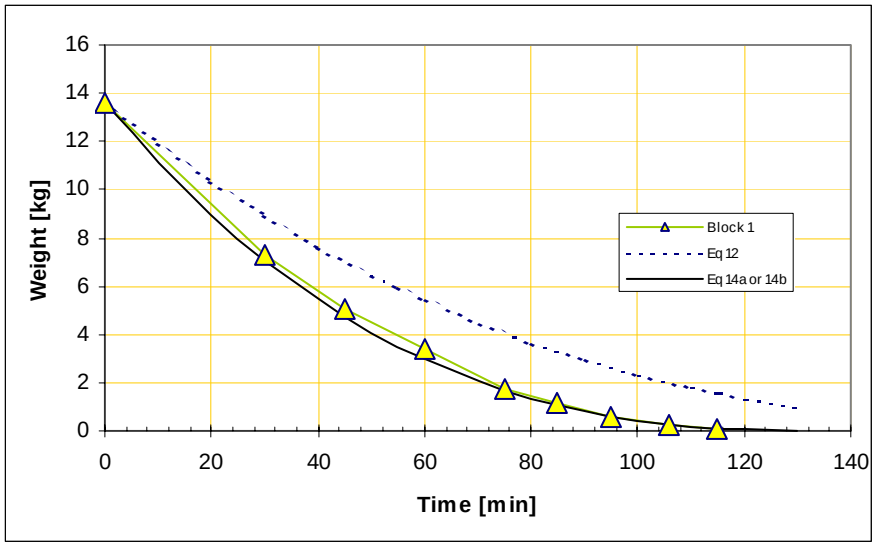

Figure 4. Measured block melting (Annex A) versus Eq.12, 14a, 14b.

3.2.4 Wave erosion

In a complementary experiment to Josberger (1977), Martin *et al*. (1977) investigated wave erosion by putting a piece of vertically faced ice in a wave tank. The development of a notch in a regular wave train of height a was measured. The notch had two zones: there was a smooth surface notch that extended about $\pm 2a$ above and below the still waterline; below about $-2a$ the notch surface extended to a depth of about $1/k$ below the still waterline, where k is the wave number. This lower surface had wavelets, or cusps.

The authors hypothesized that the notch was due to the heat transfer from the wave drift current and turbulence and concluded from a comparison of the lab results with predictions that heat transfer from wave drift current has an efficiency of about 1%. Their simple model compared well with field observations.

White *et al*. (1980) developed a prediction model based on sensible physical arguments and compared their predictions to Josberger's results and to their own pair of tests. The comparison was very good. They suggest, reasonably, that wave orbital motion will lead to a turbulent oscillating boundary layer at the ice-water interface, which will cause the ice to be eroded as heat is transferred to it from the water. This, they claim, should be a function of the wave Reynolds number and the Prandtl number. They then use wave friction on the seabed as an analogy to wave friction on any surface exposed to wave orbital paths and amplitudes, in this case an iceberg. Their model, which uses Airy wave theory, accounts for the shape and magnitude of a wave eroded surface. In their model, wave erosion is a function of the wave period and height,

the roughness of the ice, and the subsequent boundary layer friction action between the water and ice.

This model could be extended to cases where the incident waves are concentrated by the local iceberg geometry, which observations have shown can lead to accelerated erosion that can promote large scale fracturing.

An excellent example of wave erosion and its accelerated effects at local surface irregularities is given by Robe *et al*. (1976, 1977) in their report of a series of 5 full-scale aerial observations made by the IIP of an large tabular iceberg on the Grand Banks over a period of 25 days from May 12 to June 6, 1976. It was last sighted at 47°31'N, 49°07'W after having drifted across the northern entrance to the Flemish Pass. The iceberg had only 4m to 5m of freeboard and was very stable. A plot of surface area over the 25 days showed a nearly linear decrease in surface area from an initial 190,000 m^3 to 109,000 m^3. The rapid deterioration was due primarily to wave induced erosion with associated undercutting and minor calving. Surface water temperature was reported to be between 2°C and 4°C and the water temperature at about 75m to 100m was estimated to be a minimum of less than -1°C.

The visual record gives clear evidence of localized accelerated wave erosion at points around the perimeter that appear to have some initial surface irregularity. The authors concluded that a concentration of wave energy and local turbulence at these points led to progressive enlargement of small embayments. The bottom of these embayments appear to have extended only several meters below the water surface and were parallel to the water surface. The shape of the bottom of the iceberg was assumed to be flat.

The authors noted that such observations are very rare as icebergs usually change appearance rapidly due to calving, rolling, and melting so that repeated identification of the same iceberg is impossible even after a few days.

Figure 5. Outline sketches of a deteriorating tabular iceberg (after Robe *et al*. 1976).

Note that when icebergs are in pack ice, they are protected from wave erosion by the pack, which dampens wave motion. Bergs undergo more rapid wave erosion in the open sea (e.g Marko 1996).

3.3 Fragmentation Processes

3.3.1 Global cracking

The topic of natural and artificial splitting of icebergs was addressed in Diemand *et al*. (1987). The authors considered 4 sources for the stresses in icebergs (with estimated levels);

1. residual stress (remnant from glacial deformations) (≈0.1 MPa - widespread)
2. hydrostatic stresses (from the surrounding water) (small - widespread)
3. thermal stresses (arising from the heat transfer during melting) (up to 2 MPa - local)
4. buoyancy stresses on the projecting underwater rams. (≈0.5 MPa - local)

The level of residual stresses could vary widely. Stresses in glaciers are sufficient to deform the ice, although at very small strain rates. A proper estimate of the residual stresses should take the creep behavior of ice into account. In time, the residual stresses would likely all dissipate. This issue would be well served by field observations. There are methods for establishing the level of residual stresses experimentally. Whether this can be practically accomplished on an iceberg should be studied.

The hydrostatic stresses can easily be estimated. Figure 6 shows the hydrostatic stress on the base of a blocky berg (1 : 1.5 : 2) versus iceberg mass. Stresses of the order of 0.1 to 0.3 MPa are easy to achieve. These are, of course, the same stresses associated with buoyancy, although the buoyancy stresses referred to in item 4 above are actually bending stresses arising from unbalanced hydrostatic stresses.

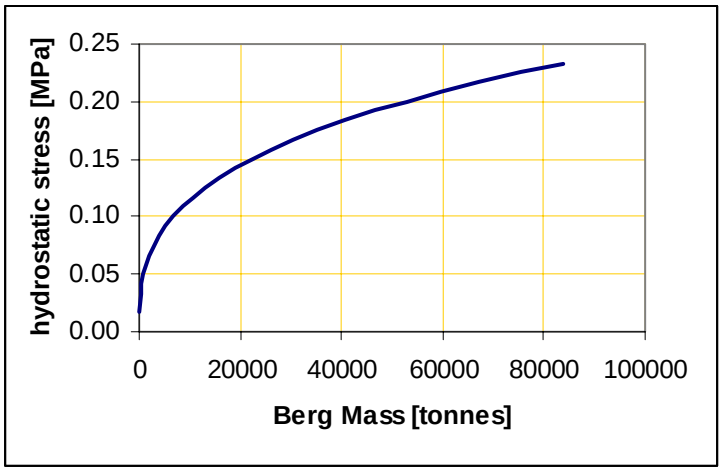

Figure 6. Maximum hydrostatic stress versus iceberg mass (assumes a 1:1.5:2 block).

One particular mechanism was postulated to explain the large fragmentation events often observed. The authors described tabular icebergs that split roughly in half. Figure 7 shows the mechanism proposed by Diemand *et al*.(1987). The relatively warm surface temperatures in the Labrador Sea in summer was postulated as the cause of enhanced waterline melting leading to the development of large underwater rams (see Figure 7). In such circumstances, bergs have been observed to split in the center with the central region of the iceberg sinking as the ends tilt up. The mechanism is a simple bending failure, in which tensile stresses exceed a limit, resulting in fracture. For the case of a particular berg, an 8 million tonne berg called Gladys, tensile stresses of 0.8MPa were estimated.

Diemand *et al*. made simple estimates of iceberg mechanical strength on the basis of grain size and strain rate. Quoting Lee and Schulson (1986) for a strain rate of 10^{-7} s^{-1}, and -10° C , a strength versus grain size equation is given as

$$\sigma = K_o d^{-0.5} \tag{15}$$

where K_o is 0.05 MPa$\sqrt{}$m. For an assumed grain size of 7.3 mm, a strength of 0.6 MPa is found, which is approximately equal to the estimated stress in Gladys.

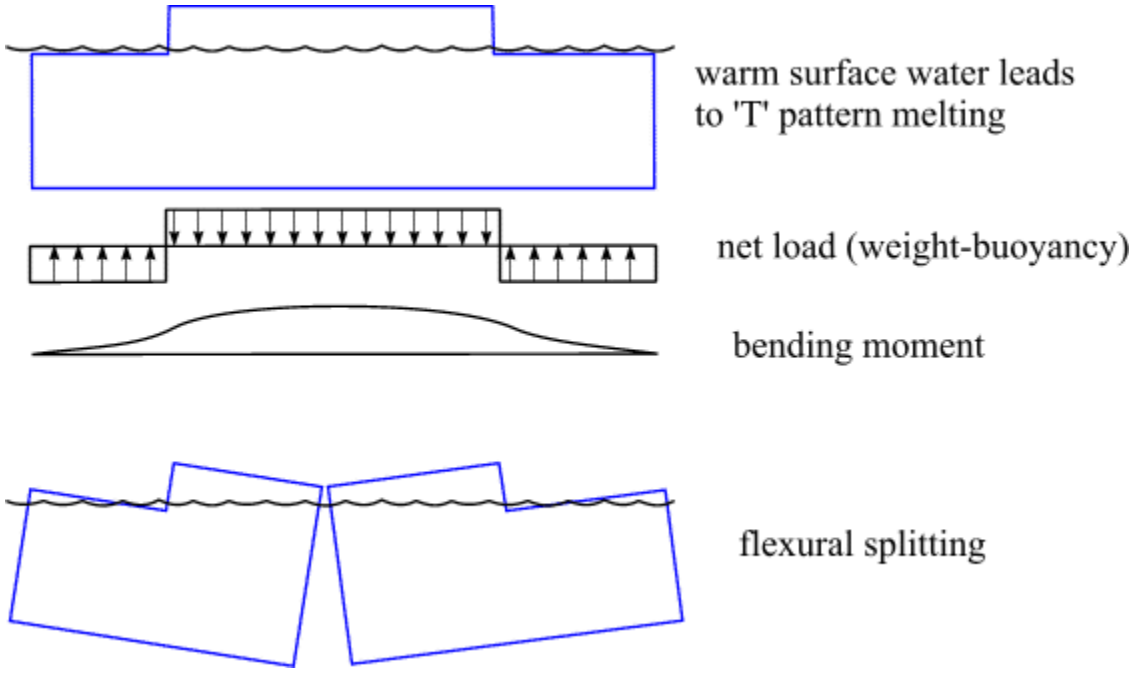

Figure 7. Tabular iceberg splitting in flexure (after Diemand *et al*. 1987).

3.3.2 Time dependent strength

The primary stresses on icebergs are sustained over a very long time, whether it be gravity, buoyancy or thermal in origin. Some stresses would be short lived, such as those due to bottom impact, wave impact or the inertial and hydrodynamic forces occurring during a roll-over event. The duration of the stress is quite important. Ice strength is a time-dependent property.

> *"The absolute values of ice strength, as well as the magnitudes 2of the ice strength parameters change from the greatest (instantaneous) values at the time of loading (t_o) to zero for longer intervals." (Fish 1991)*

In order to understand natural fragmentation processes, one must consider time dependent strength. (Note: this time dependency helps to explain why various methods to fragment ice rapidly, including the use of explosives, have tended not to work. Sustained stresses are much more effective at causing large fractures in ice.)

There are several time dependent ice strength models. Fish (1991) describes a creep model for ice strength that uses a parabolic strength model with time dependent parameters. The model assumes positive compressive stresses (i.e. may not be suitable for tensile or flexural stresses). For constant stress conditions, the shear stress at failure τ_i is given as

$$\tau_i(t) = c(t) + b(t) \cdot \sigma_m - \frac{b(t)}{\sigma_{max}} \cdot \sigma_m^2 \tag{16}$$

where $c(t)$ and $b(t) = \tan \phi(t)$ are the cohesion and friction angle, and σ_m is the mean normal stress

$$\sigma_m = \frac{\sigma_1 + \sigma_2 + \sigma_3}{3} \tag{17}$$

where $\sigma_1, \sigma_2, \sigma_3$ are the principal stresses. For relatively low confining stress, the failure criterion becomes

$$\tau_i(t) = c(t) + b(t) \cdot \sigma_m \tag{18}$$

At very low stress or strain levels, as we would have in long-term iceberg failure processes, such as natural splitting and spalling, but not collision, Fish states that strength becomes independent of confining pressure, so that we have a simple shear strength (cohesion) criterion:

$$\tau_i(t) = c(t) \tag{19}$$

Fish further states that the time dependency can be included as

$$\tau_i(t) = c_o \cdot \Phi(t) \tag{20}$$

where

$$\Phi(t) = \left(t / t_o \right)^{-1/n} \tag{21}$$

n is a parameter in the range of 3 to 5, and t_o is a time parameter equal to the lower limit of validity of creep behaviour. Fish suggests a upper strain rate limit of $\dot{\varepsilon} = 5 \times 10^{-2}$ /s. From this and the assumption that $E/\sigma = 2000$, t_o becomes;

$$t_o = \frac{1}{2000\dot{\varepsilon}} = 0.01\text{sec} \tag{22}$$

Fish reported data from (Jones 1982) for polycrystalline ice at -12°C. The exponent n =3.95 and c_o = 16.4 MPa. With this a time dependent shear strength equation (for low confining positive pressures, sustained stresses) becomes

$$c(t) = 16.4 \cdot \left(t / .01 \right)^{-1/3.95} \tag{23}$$

With time plotted in days, Figure 8 shows the declining shear strength with time. This curve is specific to the data by Jones, but is representative of the type of ice and temperatures in icebergs. The same data is plotted as strength versus strain rate in Figure 9.

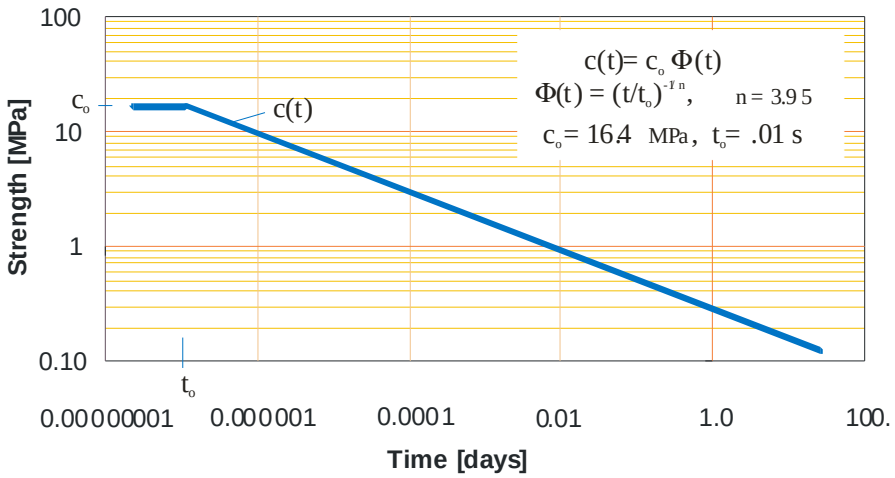

Figure 8. Time dependent shear strength for polycrystalline ice at -12°C.

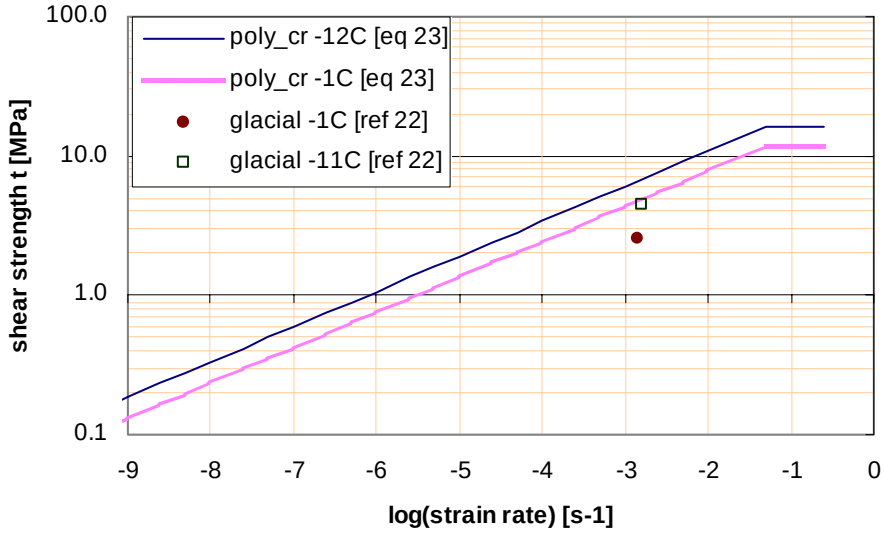

Figure 9. Shear strength versus strain rate for polycrystalline ice at -1°C, -12°C for equation 23, and data from Gagnon & Gammon (1995b).

3.3.3 Thermal cracking

Despite the relatively minor role of melting due to solar radiation, thermal stress fluctuations, which will be most severe in the above water part of an iceberg, may induce cracking, particularly local surface cracking. This ablation mechanism has received very little attention in the literature, although Robe (1980) pointed out anecdotal reports of increased cracking and calving activity coinciding with sudden increases in the amount of radiation, such as occurs on sunny mornings.

3.4 Deterioration models

Several deterioration models have been described in the literature. The most prominent are those from the International Ice Patrol (Anderson 1983) and El-Tahan *et al*. (1984), which are aimed at complementing drift models.

The IIP deterioration model (Anderson 1983) is based entirely on work done by White *et al*. (1980) and includes four deterioration mechanisms: insolation, buoyant natural convection, underwater forced convection, and wave erosion. Air convection and fragmentation processes, including calving due to wave erosion are ignored. Using the model, the sum of the deterioration components are summed and the total deterioration is calculated as a percentage of the starting size of an iceberg. As IIP usually does not collect any detailed information on iceberg size or geometry, but rather only on approximate size classification (i.e. growler, small, medium, large), the starting lengths are somewhat arbitrarily assigned lengths that are deemed to be characteristic of the iceberg's estimated size class. Clearly, the purpose of the model is to make gross estimates of the expected change in size of a multitude of iceberg targets, rather than give anything approaching a detailed account of a particular iceberg's evolution.

Hanson (1988) explained that the IIP parametric forecast model of iceberg deterioration, in conjunction with its dynamic drift model (Mountain 1980), is used to complement their primary role in identifying iceberg threats by helping to establish positive iceberg resights and to eliminate targeted icebergs from their forecasted drift. This is especially important when intervals between observations are long. The author reported a field study that was undertaken to critique the IIP deterioration model, with particular emphasis on checking the accuracy of environmental input data. This work illustrates the importance of accurate input data.

Six medium icebergs were observed by ship for up to 6 days near 50°45′N 53°30′W. In situ environmental data were collected and the IIP model was used to make predictions using both the its normal 'global' environmental inputs and the in situ data. Based on a comparison of the results Hanson concluded that while the modeled insolation was likely to be off by 100%, the relative insignificance of this component and the difficulty of acquiring and incorporating detailed insolation data in the model was not worthwhile. Likewise, the effect of using surface water temperature in the model was compared with using more precise water temperature measurements at depth. Using surface temperature was found likely to result in overestimation of both buoyant and forced convection by a factor of about 3. This error would only occur in summer when the sea temperature was warm enough to cause melting. Unfortunately, the author says that deeper water temperatures are not easy to get and the status quo is good enough. With

respect to forced convection in terms of the effect of the relative motion between the iceberg and water, the IIP model use of historical current data to judge water speed, and its neglect of wind driven current was found to lead to significant error that could be put right by incorporating wind driven current, which is used in the drift model. The most important component in the model, wave erosion, was found to be over predicted by the IIP model because of the global wave data inputs were over predicted. This could be addressed by using better wave climate prediction models.

Very little is reported about the actual iceberg observations. While the observation period was not long, the presence of growlers and bergy bits near the icebergs indicated that they were in a state of rapid deterioration. One iceberg was observed to roll over, which resulted in its height doubling and its waterline length increasing by about 5%. Changes in the above water shape of several other icebergs indicated that they too had rolled, although they were not observed doing so. Remarkably, the author made no recommendations that fragmentation processes be modeled in future.

El-Tahan *et al*. (1984) provide a detailed account of their iceberg deterioration model, which derives strongly from White *et al*. (1980) and has been used in a series of subsequent publications, some of which are discussed below. The model is exercised for three cases and comparisons are made with corresponding field observations. Two of the field observations (Kollmeyer 1965 and Robe *et al*. 1977) are in the open literature, the third is not. The authors show that wave erosion and calving associated with wave erosion is the most important deterioration mechanism, accounting for more than 80% of the mass loss. Melting due to forced convection is significant at about 16%, which is about 8 times the melting rate due to natural buoyant convective melting. Insolation and wind convection account for less than 0.5% each. The authors say that underwater fragmentation of shelves, accelerated erosion and cracking at flaws, and thermal stress cracking are practically impossible to model and these omissions might explain differences between observed and predicted deterioration.

Venkatesh *et al*. (1985) reported results from a detailed 15 day field study of 2 grounded bergs (1.6×10^6 and 0.8×10^6 tonnes) off St. John's. The fact that the icebergs were grounded close to shore made local measurements of environmental conditions and observations of local deterioration practical, which is not often the case. A comparison with an iceberg deterioration model (El-Tahan *et al*. 1984) was made and found to underestimate mass losses by about 10% in one case, and substantially more in the second case. The authors attributed the relatively poor comparison in the second case to difficulties associated with the change in iceberg orientation during the observation period, which they claimed introduced errors in estimates of mass changes, although it would seem that such uncertainties existed regardless of iceberg orientation.

Another suggested reason for the poor comparison was that other mass loss mechanisms that were not modeled, such as thermal cracking, caused more rapid deterioration than predicted. In the first case, the model indicated that 88% of the mass loss was due to wave erosion and the associated calving from overhangs, 9% due to forced water convection, 2% due to buoyant convection, and 0.5% each due to wind convection and insolation. The authors also provided a brief review of previous deterioration work, going back to 1912.

Venkatesh (1986) picked up one of the loose threads from Venkatesh *et al*. (1985) by pursuing an explanation of the poor comparison between modeled and observed results of the deterioration of a 0.8×10^6 tonne iceberg, the second of the two icebergs studied previously. Consideration is given to how grounding might affect estimates of iceberg mass and deterioration rate, especially in light of the reorientation of the observed iceberg, although the results do not add significantly to the original paper.

Venkatesh and El-Tahan (1988) undertook work to determine how melting affected iceberg distributions. This is similar in intent to the IIP's use of a deterioration model, although the authors apply a more detailed characterization of icebergs by category than do the IIP.

Venkatesh *et al*. (1994) exercised El-Tahan *et al*.'s (1984) deterioration model in connection with a field study of iceberg drift in sea ice. The main aim of the field work was to investigate the effect of sea ice on iceberg drift for IIP drift model validation, although Mountain's (1980) model does not contain a sea ice force term. To do so, two medium tabular icebergs were instrumented and tracked using satellites for more than a month in the marginal ice zone at about 51° to 52°N offshore Newfoundland and Labrador. The ice concentration was about 9/10s at the start of the field work and changed to 3/10s before the work was complete. Interestingly, the drift model seemed to do as well in broken sea ice as in open water, indicating that broken ice, even in high concentration, does not have a large impact on drift. In terms of deterioration, the remote location of the icebergs precluded anything approaching continuous observation of local deterioration processes, so the comparison of predicted with actual results requires a certain amount of inference. The temperature and wave height inputs, which are important in the dominant wave erosion and calving deterioration terms, were based on reasonable estimates, although not always direct measurements on site.

3.5 Iceberg shape

Icebergs evolve into unusual shapes that defy simple categorization, although the size and shape categories that have been defined by the IIP and the World Meteorological Organization (1970) are widely used for descriptive purposes.

Three size categories are given by the WMO: icebergs, bergy bits, and growlers. An iceberg is defined as a massive piece of glacial ice whose above water volume, or sail, extends at least 5 m above the waterline and has a water plane area greater than 300 m^2. The sail of a bergy bit extends between 1 m and 5 m above the waterline and has a water plane area of about 100 to 300 m^2. The smallest size category is growler and this refers to a piece of glacial ice that extends less than 1 m above the waterline and has a water plane area of about 20 m^2.

The IIP size categories shown in Table 5 are roughly the same, but they further divide the iceberg category into small, medium, large, and extra large sizes. IIP size and shape classifications have changed over the years in response to detection methods.

Table 5. IIP iceberg size categories (IIP website).

Category	Height [m]	Length [m]
Growler	< 1	< 5
Bergy Bit	1-4	5-14
Small	5-15	15-60
Medium	16-45	61-122
Large	46-75	123-213
Very Large	> 75	> 213

The IIP also has shape categories: tabular and non tabular. Non tabular shapes include blocky, pinnacle, dry dock and dome. Tabular icebergs have horizontal or flat tops with a maximum waterline length to sail height ratio greater than 5:1. The largest icebergs are tabular. Blocky icebergs are steep sided and flat topped with a length to height ratio of about 2.5:1. Pinnacle icebergs are characterized by a central spire or a pyramid shape that may have several spires. Drydock icebergs have a wave eroded U-shaped slot between two or more columns or pinnacles. Dome icebergs are smooth and rounded with low sides (e.g. Robe 1980). Venkatesh & El-Tahan (1988) added estimates of perimeter, mass, and surface area to average size classifications as shown in Table 6.

Table 6. Average iceberg size (after Venkatesh & El-Tahan 1988).

Category	Length [m]	Mass (tonnes)	Perimeter [m]	Wetted surface area [m^2]	Total surface area [m^2]
Growler (non tabular)	10	450	30	250	350
Small (non tabular)	55	75,000	155	8,000	10,300
Medium (non tabular)	125	900,000	360	36,000	48,000
Large (non tabular)	225	5,500,000	650	110,000	150,000
Small (tabular)	80	250,000	235	15,000	20,000
Medium (tabular)	175	2,170,000	500	67,000	92,000
Large (tabular)	260	8,230,000	750	150,000	204,000

A number of field studies of iceberg size, shape, and other characteristics have been carried out over the years on the Grand Banks and Labrador Sea, many in connection with oil and gas industry activities. A recent report (Anon. 1999), sponsored by the Program for Energy Research and Development (PERD), has compiled much of the information from over 40 reviewed reports, including data that has previously been confidential, into a single database. The main aim of the compilation effort was to get a better idea of iceberg shape in order to better inform the estimation of iceberg impact loads for offshore installation design. The database includes dimensions for 872 icebergs, detailed 3-dimensional sonar profile information on the underwater portion of 28 icebergs, detailed 3-dimensional information on 566 iceberg sails from stereo photography, and 2-dimensional profiles of 155 iceberg sails and keels. This is a very useful source of field measurements and complements the iceberg sightings statistics reported by Singh *et al*. (1998). The authors also did a simple analysis of the length, width, height, draft, and mass data that they compiled, and reported results such as length versus draft relationships. Some earlier attempts to find meaningful relationships between above water parameters and draft were not successful (e.g. Buckley *et al*. 1985).

The database contains significantly more 3-d above water iceberg data (from stereo pictures) than 3-d underwater data (sonar profiles). The authors make the bold assumption that the above and under water shapes are statistically similar, based on the premise that icebergs roll frequently, although this is not justified by the authors. Such an assumption cannot go unchallenged and should be addressed.

In a subsequent study, some of the 3D data were compiled into a visualization database (Barker *et al*. 1999). This included 52 sail and 25 keels. In only 3 cases were both sail and keel data available.

3.5.1 Shape definition

The choice of method of representing the natural surfaces of icebergs is directed by the need for flexibility to describe the shape, keep track of and update shape changes, determine hydrostatic, floatation, and stability characteristics, and evaluate stresses.

Right handed Cartesian coordinate systems are used here. A set of inertial, or space axes, denoted x_o, y_o, z_o is fixed with respect to the undisturbed water surface with the z_o axis pointed down. A non inertial, or body, axes system x, y, z is fixed to the iceberg body. As the iceberg shape evolves, the axes will reorient itself with the iceberg as it moves to maintain static equilibrium, but its initial origin position can be chosen for convenience. The position and orientation of the body axes with respect to the space axes is given by the Cartesian coordinates (x_o, y_o, z_o) measured in the direction of the x_o, y_o, z_o axes, respectively, and by the Eulerian angles (Φ, Θ, Ψ). For example, the position of the origin O of the iceberg body axes with respect to the inertial system is

$$\mathbf{R}_O = \{x_O, y_O, z_O\}^{\mathrm{T}} \tag{24}$$

where the right hand side is the column matrix representation of the vector, as indicated by the transpose T.

The surface is defined by a series of points (x, y, z) in the body system and a surface unit normal vector $\hat{\mathbf{n}}$ into the body at each point. Each surface point is explicitly associated with two nearby points to form a triangular surface plane: unit tangents from the surface point to its two associated points define the surface normal. The set of elemental triangular areas constitute the discretized surface area. Changes in shape due to continuous ablation processes are evaluated at each point at specified time intervals; likewise the surface normals are evaluated at each point using the new positions of the surface points. As the ablation processes involve a variety of environmental conditions that are more or less directional, it is necessary that the vectors defined in the body system be known in the inertial system as well. This can be done with the appropriate coordinate system transformation, which is described in detailed below.

The surface geometry representation described above is robust and easily adaptable to several software platforms. The initial geometry must be explicitly defined and subsequent continuous changes can be handled automatically. Discrete fragmentation events and the resulting geometry changes are handled separately.

3.5.2 Coordinate system transformation

The orientation of a body axes relative to an inertial axes is given by three consecutive rotations through the Eulerian angles (Φ, Θ, Ψ). The coordinate transformation method used here follows Abkowitz (1969) and Kalske (1993). In Figure 10, a body axes system x_1, y_1, z_1 is shown with its initial orientation equal to some fixed axes (which for convenience can be assumed to be coincident with x_1, y_1, z_1. The first rotation is about the z_1 axis through an azimuth angle Ψ; the rotated body axes become x_2, y_2, z_2. The rotation matrix $\mathbf{T}(\Psi)$ is given in Eq.25.

$$\mathbf{T}(\Psi) = \begin{bmatrix} \cos\Psi & \sin\Psi & 0 \\ -\sin\Psi & \cos\Psi & 0 \\ 0 & 0 & 1 \end{bmatrix}. \tag{25}$$

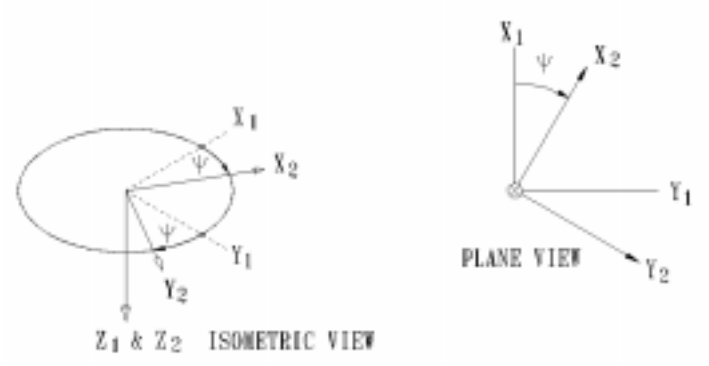

Figure 10. Rotation of body axes through azimuth angle Ψ.

The second rotation is about the y_2 axis through the trim angle Θ, as illustrated in Figure 11. The rotated body axes become x_3, y_3, z_3. Its transformation matrix T(Θ) is

$$\mathbf{T}(\Theta) = \begin{bmatrix} \cos\Theta & 0 & -\sin\Theta \\ 0 & 1 & 0 \\ \sin\Theta & 0 & \cos\Theta \end{bmatrix}. \tag{26}$$

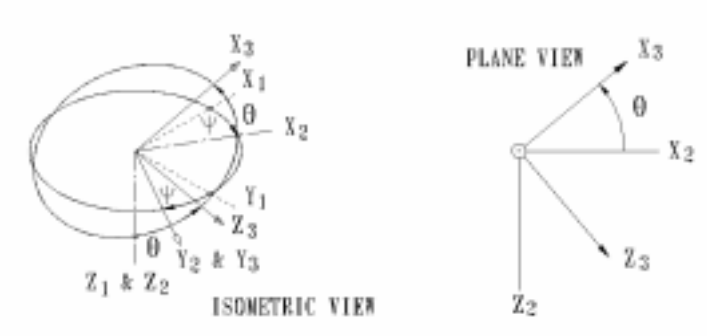

Figure 11. Rotation of body axes through trim angle Θ.

The third rotation is about the x_3 axis through the roll angle Φ, as shown in Figure 12 where the *x, y, z* axes give the final orientation of the body with respect to the space axes x_o, y_o, z_o. Its rotation matrix is $\mathbf{T}(\Phi)$, written as

$$\mathbf{T}(\Phi) = \begin{bmatrix} 1 & 0 & 0 \\ 0 & \cos\Phi & \sin\Phi \\ 0 & -\sin\Phi & \cos\Phi \end{bmatrix}. \tag{27}$$

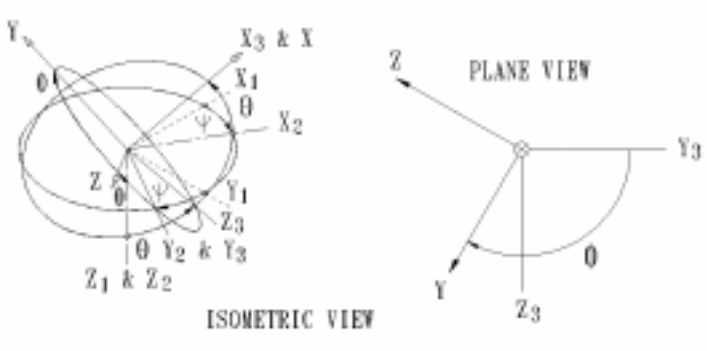

Figure 12. Rotation of body axes through roll angle Φ.

These three rotations must be done in this order to arrive at the required body axes orientation. The rotation matrices can be combined to give the transformation matrix $\mathbf{T}_T$:

$$\begin{aligned} \mathbf{T}_T &= \mathbf{T}(\Phi)\mathbf{T}(\Theta)\mathbf{T}(\Psi) \\ &= \begin{bmatrix} \cos\Theta\cos\Psi & \cos\Theta\sin\Psi & -\sin\Theta \\ \sin\Phi\sin\Theta\cos\Psi - \cos\Phi\sin\Psi & \sin\Phi\sin\Theta\sin\Psi + \cos\Phi\cos\Psi & \sin\Phi\cos\Theta \\ \cos\Phi\sin\Theta\cos\Psi + \sin\Phi\sin\Psi & \cos\Phi\sin\Theta\sin\Psi - \sin\Phi\cos\Psi & \cos\Phi\cos\Theta \end{bmatrix} \end{aligned} \tag{28}$$

where the subscript T denotes that this transformation is for translational velocity, position, and force vectors. The inverse of this transformation is $\mathbf{T}_T^{-1}$, given by

$$\mathbf{T}_T^{-1} = \begin{bmatrix} \cos\Theta\cos\Psi & \sin\Phi\sin\Theta\cos\Psi - \cos\Phi\sin\Psi & \cos\Phi\sin\Theta\cos\Psi + \sin\Phi\sin\Psi \\ \cos\Theta\sin\Psi & \sin\Phi\sin\Theta\sin\Psi + \cos\Phi\cos\Psi & \cos\Phi\sin\Theta\sin\Psi - \sin\Phi\cos\Psi \\ -\sin\Theta & \sin\Phi\cos\Theta & \cos\Phi\cos\Theta \end{bmatrix}. \qquad (29)$$

To illustrate the utility of the coordinate system transformation and the inverse transformation, consider the position vector $\mathbf{r}_P$, which locates a point P on a body's surface and whose components are given in its body axes. Given the position in space of the body axes' origin by $\mathbf{R}_O$, and the orientation angles (Φ,Θ,Ψ), the position vector in the space axes of the point P is given by $\mathbf{R}_P$:

$$\mathbf{R}_P = \mathbf{R}_O + \mathbf{T}_T^{-1}\mathbf{r}_P \,. \qquad (30)$$

The components of a vector given in the space coordinate system are determined in a body coordinate system oriented at angles (Φ,Θ,Ψ) to the space axes by the transformation matrix in Eq.28. The inverse transformation is applied in the opposite case, such as in Eq.30, when components of a vector given in a body axes system are to be determined in the space axes.

3.5.3 Hydrostatics and stability

Evaluation of the hydrostatic, floatation, and stability properties of an arbitrarily shaped floating body is not trivial. Some attempts have been made to set simple stability criteria for iceberg shapes using information that can be estimated from the above water portion of the iceberg (e.g. Weeks & Mellor 1977, Bass 1980). The approach taken here is based on integration of pressure over the elemental areas that make up the iceberg's surface (see e.g. Patel & Witz)..

First, the volume and center of mass of the body must be determined. The body is assumed to be of constant density so the centroid of the volume is equivalent to the center of mass. If the body is completely submerged, the integrated pressure over the surface S that encloses the volume V will give the buoyancy force $\mathbf{F}_B$, but this force will be greater than the weight of the iceberg since $\rho_I < \rho_w$. On an elemental area ds the pressure is

$$d\mathbf{F} = \rho_w g z \cdot \hat{\mathbf{n}} ds \tag{31}$$

where z is the vertical depth from the free surface of the center of the area ds and $\hat{\mathbf{n}}$ is a unit normal vector into the body. Integration gives

$$\mathbf{F} = \rho_w g \iint_S z \cdot \hat{\mathbf{n}} ds \tag{32}$$

or since the interest here is in the buoyancy force

$$\mathbf{F}_B = \rho_w g \iint_S z\hat{\mathbf{k}} \cdot \hat{\mathbf{n}} ds \tag{33}$$

which Archimedes tells us is equal to the weight of the water displaced so that

$$\begin{aligned} V &= \iint_S z\hat{\mathbf{k}} \cdot \hat{\mathbf{n}} ds \\ &= \iiint_V dV \end{aligned} . \tag{34}$$

The weight of the iceberg can then be found from

$$\mathbf{F}_W = \rho_i g \iint_S z\hat{\mathbf{k}} \cdot \hat{\mathbf{n}} ds . \tag{35}$$

The Eq.34 above is an example of the divergence theorem:

$$-\oiint_S \hat{\mathbf{f}} \cdot \hat{\mathbf{n}} ds = \iiint_V \nabla \cdot \hat{\mathbf{f}} dV \tag{36}$$

where $\hat{\mathbf{f}}$ is a vector and $\hat{\mathbf{n}}$ is as before a unit normal vector to an elemental area ds of a piecewise continuous surface S that encloses a volume V. The divergence theorem can be applied to determine the centroid of the volume, which as noted above is equivalent to the center of gravity CG when density is constant. For example, the vertical coordinate z_{CG} can be found by recognizing that

$$z_{CG} = \frac{1}{V}\iiint_V z\hat{\mathbf{k}}dV = -\frac{1}{V}\oiint_S \frac{z^2}{2}\hat{\mathbf{k}}\cdot\hat{\mathbf{n}}ds\,. \tag{37}$$

The coordinates in the horizontal plane can be found in a similar way, which is preferred, or by taking moments of the elemental buoyancy forces

$$\mathbf{r}_{CG(x,y)} = \frac{1}{V}\iint_S \mathbf{r}\times z\hat{\mathbf{k}}\cdot\hat{\mathbf{n}}ds \tag{38}$$

where the coordinates are measured from the origin of a coordinate system fixed at the free surface with its *z* axis pointing down. In general, care must be taken to ensure that the appropriate axes system representation of all vectors has been chosen. This is especially important when the body axes are arbitrarily oriented with respect to the inertial axes.

The next problem is to determine the equilibrium position or positions that the arbitrarily shaped body can assume. There are two possible approaches to this problem, one being the conventional use of metacentre and the other based on potential energy considerations (e.g. Bass & Peters 1984, Lever *et al*. 1991, Lewis & Bennett 1984, Benedict 1980). The energy approach is used here because it lends itself to a thorough evaluation of the iceberg's possible stable orientations, which is useful information because the greater the number of possible stable orientations, the more likely the iceberg is to roll.

For a given orientation, the waterline position at which the static equilibrium condition

$$\mathbf{F}_W = \mathbf{F}_B \tag{39}$$

is satisfied can be found by iteration. The iteration routine can be based on volume, that is, by finding the position at which the ratio of underwater volume to total volume is equal to the ratio of iceberg density to water density, or it can be done directly by integrating the pressure on the underwater surface until the buoyancy is equal to the known weight. A quite different approach was proposed by McKenna *et al*. (1999). In order to reduce the computational effort required by the above approaches, they randomly distributed a large number of point masses throughout the enclosed volume and then used these points as the basis for hydrostatic calculations. Once the

position at which Eq.39 is satisfied is determined within some predefined error limit, the center of buoyancy CB can be determined.

The above condition alone does not necessarily satisfy stability requirements, nor even equilibrium because it does not ensure that the centers of mass and buoyancy are in the same vertical line, nor, if they are, that the equilibrium position is stable, unstable or neutral. However, if this process is repeated over a range of body orientations, then a map of potential energy as a function of orientation angles can be determined. Bass & Peters (1984) noted that 2° to 5° increments in orientation was adequate for the 2 dimensional bodies they considered. Potential energy is proportional to the vertical distance between the centers of gravity and buoyancy, $\overline{BG}$.

$$E(\Theta,\Phi) = \rho_i g V \overline{BG} \tag{40}$$

Equilibrium positions occur at relative minima.

Bass & Peters (1984) and Lewis & Bennett (1984) used the potential energy approach to study the orientation stability of 2 dimensional bodies of constant density. The former authors illustrated nicely how melting can affect stability, although melting was not actually modeled. In both cases, the concern was the change in draft due to changes in orientation. The former authors showed that increases of up to 50% could occur and that an average increase of 25% could be expected. The latter authors found the draft changes to be a more modest 20% and that decreases in draft were as likely as increases.

Lever *et al*. (1991) extended Bass & Peters' (1984) model to 3 dimensional iceberg shapes for the purpose of investigating scouring events. The authors described the Dynamics of Iceberg Grounding and Scouring (DIGS) experiment off Labrador in 1985, during which detailed field measurements and observations of two iceberg grounding events were recorded. Above water and underwater records of iceberg shape were made and these were used to model and calculate 3D hydrostatic stability maps. One iceberg, Bertha, calved while grounded and then rolled. Its roll caused pitting of the seabed. Another iceberg, Gladys, had a moderate calving event and reoriented itself by 10° to 15°. After 15 minutes it split in half. One half rolled 30° and grounded. The post split roll was a high energy event. Both of these icebergs were instrumented for motions. A third iceberg, Frieda, was not instrumented, but was observed to have large underwater shelves from which it calved twice and then split in half.

4 Modeling Approaches

The authors intend to develop numerical models of iceberg evolution. A variety of numerical approaches might be taken, including finite-element, discrete element, boundary element, finite difference and lattice models. All of these methods are capable of modeling the continuum behaviour of the interior of an iceberg. However, at this early stage, two simpler approaches are being contemplated. Rather than model the internal structure as a continuum, a model that assumes rigid behaviour will be explored. The melting process will modify the rigid body shape. Fracture will be assumed to be the result of the formation of a failure plane, dependent on the gross stress on the plane. A 2D implementation of the concept is sketched in Figures 13 and 14.

The 2D model would contain melting and wave erosion algorithms, in which the surface patches would migrate inwards. The spalling would be modeled as through-body fracture events, along one of a finite set of lines joining edge nodes. The failure criteria would be a time-based shear criteria, along the lines discussed by Fish (1991) (e.g. Eq.23). At each time step the rigid body hydrostatic equilibrium would be solved to find the body position and orientation. At each time step the stress on each candidate failure plane will be determined. The failure criteria will be time sensitive, so a cumulative measure of stress will be needed. The complete model will include the melt, stability and spalling behavior.

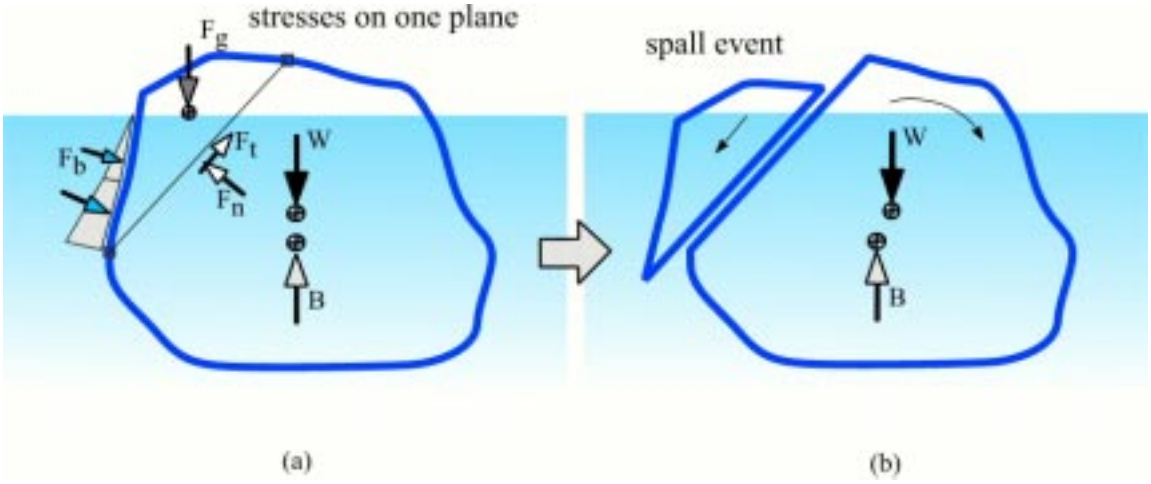

Figure 13. Concept of 2D (prismatic) model of iceberg evolution model.

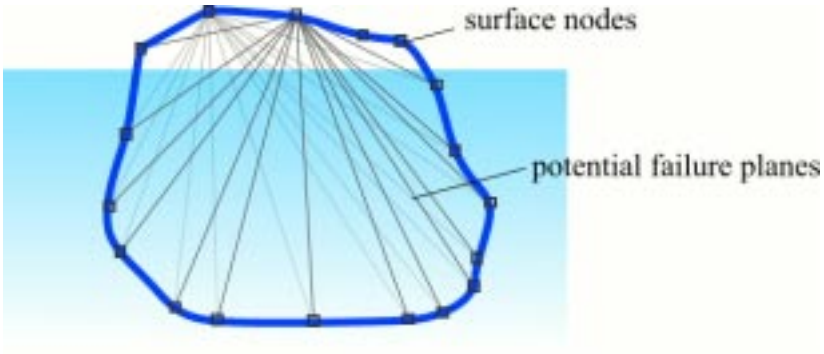

Figure 14. Potential failure planes in the 2D model.

The 2D model can potentially be extended to 3D by extending the surface description from segments to patches. The simple failure planes will be extended to candidate failure surfaces, each made up of a set of failure surface patches. The melting and failure criteria will be essentially the same, as will the hydrostatic stability. Figure 15(a) illustrates the surface patches and candidate spalls on a 3D model. Figure 15(b) illustrates the nature of the failure surface. With each spall, the ice body will have part of the surface re-meshed. Some adaptive meshing scheme may be needed as the shape changes.

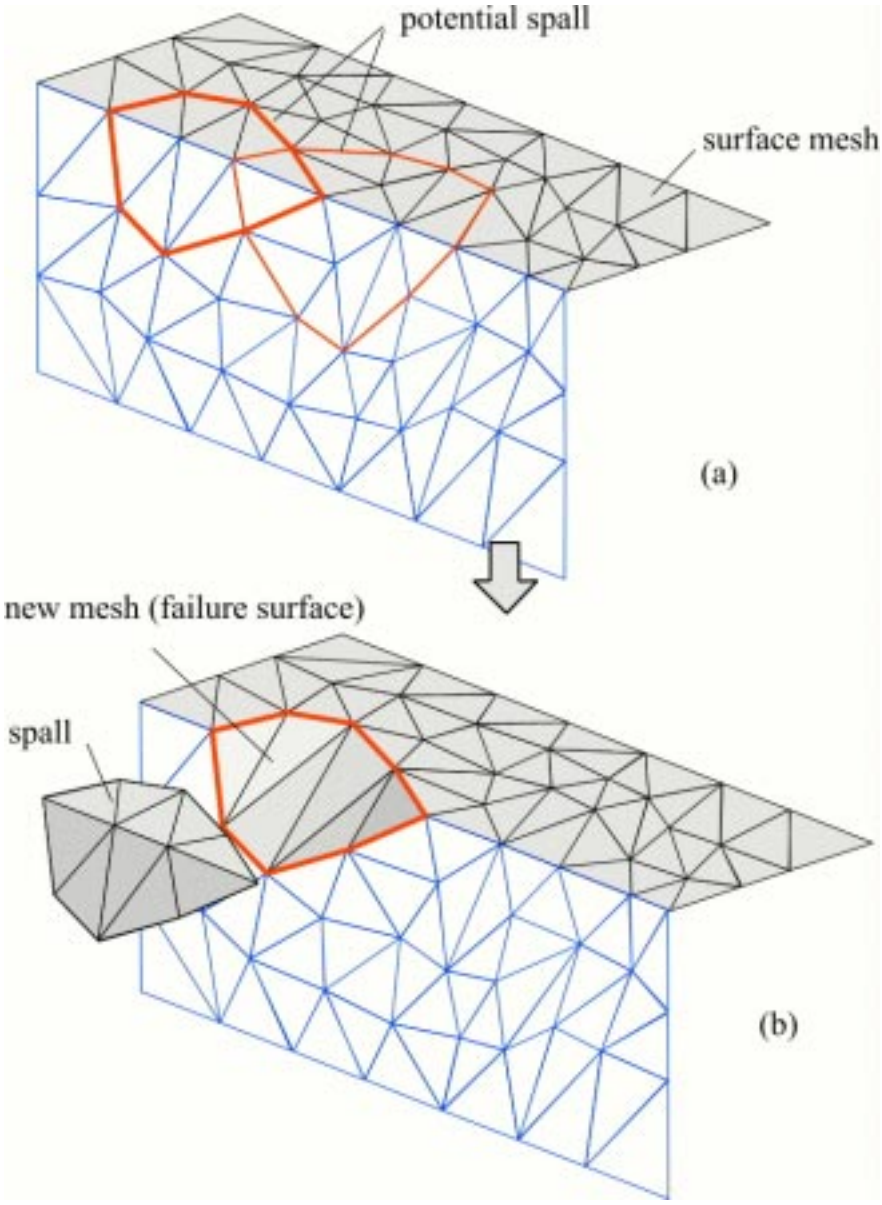

Figure 15. Concept for a 3D rigid-body, melting, spalling ice evolution model.

Figures 16, 17 and 18 show photographs of icebergs near Newfoundland. The photos show both smooth (melted) and broken (spalled) surfaces. The aim of the modeling work is to be able to reproduce and explain the specific origin of such shapes.

Figure 16. Iceberg off Tors cove, Newfoundland, 1991.

Figure 17. Iceberg 2 (looking North) in Conception Bay, Newfoundland, 1991.

Figure 18. Iceberg 2 (looking East) in Conception Bay, Newfoundland, 1991.

5 Conclusions

The report has examined some of the fundamental features and mechanics of icebergs. The report is a starting point to develop iceberg evolution models that will include the main processes that alter the iceberg's shape. Surface melting is a continuous process, while spalling and rolling are discrete events that result in near-instantaneous changes in the effective (presented) shape of an iceberg. Iceberg shape is the key input for both motion and collision predictions. The proposed models will move a significant step towards realistic models of the evolving shape of icebergs.

Iceberg evolution is a complex combination of interacting deterioration processes. At present, there is no model that incorporates the deterioration processes with a detailed account of iceberg shape evolution, which is what the authors have taken the first steps towards in this work. A crucial component of this approach is the accurate treatment of hydrostatics, floatation, and stability.

Initially, existing models of thermodynamic ablation processes can reasonably be adopted and used for shape evolution modeling. However, the most important of these, wave erosion, should be validated with full scale observations and extended to include accelerated local erosion due to concentration of incident waves. We propose that the stress concentrations that result can cause large scale fragmentation, in combination with hydrostatic and wave induced loads, and with inertial loads during instability events. The state of knowledge concerning iceberg fragmentation is relatively weak.

In the first instance, this will be a deterministic model, and will subsequently be extended to incorporate a probabilistic treatment of environmental conditions, including iceberg motions, and fracture initiation flaws. Eventually, we see this integrating with an ocean circulation model capable of large scale and local scale modeling so giving a coupled drift - deterioration model.

6 References

1. Abkowitz, M.A.. 1969. Stability and motion control of ocean vehicles. MIT Press, Cambridge, 253 pp.
2. Anderson, I. 1983. Iceberg deterioration model. In Report of the International Ice Patrol Service in the North Atlantic, U.S. Coast Guard Bulletin No.69, CG-188-38, pp.67-73.
3. Anderson, I. 1993. International Ice Patrol iceberg sighting database 1960-1991. Report of the International Ice Patrol Service in the North Atlantic, U.S. Coast Guard Bulletin No.62, CG-188-48.
4. Anon. 1999. Compilation of iceberg shape and geometry data for the Grand Banks region. Canatec Consultants Ltd. and others for PERD/CHC Report 20-43, 37 pages + appendices.
5. Anon. 1970. WMO sea ice nomenclature. World Meteorological Organization, No.259.TP.145, Geneva.
6. Bader, H. 1977. A critical look at the iceberg utilization project. Proceedings Iceberg Utilization, A.A.Husseiny (ed.), Pergamon Press, pp.34-44.
7. Banke, E.G. and Smith, S.D. 1974. Measurements of towing drag on small icebergs. Proc. IEEE International Conference on Engineering in the Ocean Environment, Halifax, Vol.1, pp.130-132.
8. Bass, D.W., and Peters, G.R. 1984. Computer simulation of iceberg instability. Cold Regions Science and Technology, Vol.9, pp.163-169.
9. Bass, D.W. 1980. Stability of icebergs. Annals of Glaciology, Vol.1, pp.43-47.
10. Bigg, G.R., Wadley, M.R., Stevens, D.P., and Johnson, J.J. 1997. Modeling the dynamics and thermodynamics of icebergs. Cold regions Science and Technology, Vol.26, pp.113-135.
11. Bigg, G.R., Wadley, M.R., Stevens, D.P., and Johnson, J.A. 1996. Prediction of iceberg trajectories for the North Atlantic and Arctic Oceans. Geophysical Research Letters, Vol.23, No.24, pp.3587-3590.
12. Bindschadler, R.A. and Rasmussen, L.A. 1983. Finite-difference model predictions of the drastic retreat of Columbia Glacier, Alaska. Geological Survey Professional Paper 1258-D, 17 pp.
13. Brown, C.S., Meier, M.F., and Post, A. 1982. Calving speed of Alaska tidewater glaciers, with application to Columbia Glacier. Geological Survey Professional Paper 1258-C, 13 pp.

14. Daley, K., Ice Block Melting Project, Bishops College, Feb. 2000.

15. Diemand, D., Nixon, W.A., and Lever, J.H. 1987. On the splitting of icebergs, natural and induced. Proc. OMAE, Vol.IV.

16. Dowdeswell, J.A., Whittington, R.J., and Hodgkins, R. 1992. The sizes, frequencies, and freeboards of East Greenland icebergs observed using ship radar and sextant. Journal of Geophysical Research, Vol.97, No.C3, pp.3515-3528.

17. El-Tahan, H.W., El-Tahan, M., and Venkatesh, S. 1983. Factors controlling iceberg drift and design of an iceberg drift prediction model. Proc. POAC, Vol.3, pp.263-281.

18. El-Tahan, M., Venkatesh, S., and El-Tahan, H. 1984. Validation and quantitative assessment of the deterioration mechanisms of Arctic icebergs. Proceedings, Offshore Mechanics and Arctic Engineering, Vol.3, pp.18-25.

19. Fish, A. M. 1991. Creep and yield model of ice under combined stress" CRREL Special Report 91-31, Hanover, New Hampshire.

20. Fuglem, M., Jordaan, I., Crocker, G., Cammaert, G., and Berry, B. 1996. Environmental factors in iceberg collision risks for floating systems. Cold Regions Science and Technology, Vol.24, pp.251-261.

21. Gagnon, R.E. and Gammon, P.H. 1995a. Characterization and flexural strength of iceberg and glacier ice. Journal of Glaciology, Vol.41, No.137, pp.103-111.

22. Gagnon, R.E. and Gammon, P.H. 1995b. Triaxial experiments on iceberg and glacier ice. Journal of Glaciology, Vol.41, No.139, pp.528-540.

23. Gammon, P.H., Gagnon, R.E., Bobby, W., and Russell, W.E. 1983. Physical and mechanical properties of icebergs. Proceedings Offshore Technology Conference, pp. 143-150.

24. Garrett, C. 1985. Statistical prediction of iceberg trajectories. Cold Regions Science and Technology, Vol.11, 255-266.

25. Gaskill, H.S. and Rochester, J. 1984. A new technique for iceberg drift prediction. Cold Regions Science and Technology, Vol. 8, pp.223-234.

26. Hanson, W.E. 1988. Operational iceberg forecasting concerns. Proceedings, Oceans, Vol.2, pp.561-566.

27. Hill, B.T. 1999. Historical record of sea ice and iceberg distribution around Newfoundland and Labrador, 1810-1958. Proc. OMAE, ASME, 7 pp.

28. Hobbes, P.V. 1974. Ice physics. Clarendon Press, Oxford, 837 pp.

29. Holdsworth, G. 1973. Ice calving into the proglacial Generator Lake, Baffin Island, N.W.T., Canada. Journal of Glaciology, Vol.12, No.65, pp.235-250.

30. Holdsworth, G. 1977. Some mechanisms for the calving of icebergs. Proceedings Iceberg Utilization, A.A.Husseiny (ed.), Pergamon Press, pp.160-175.

31. Isaacson, M. and McTaggart, K. 1990. Modelling of iceberg drift motions near a large offshore structure. Cold Regions Science and Technology, Vol.19, pp.47-58.

32. Johannessen, K., Løset, S., and Strass, P. 1999. Simulation of iceberg drift. Proc. POAC, pp.97-105.

33. Jones, S.J. 1978. Triaxial testing of polycrystalline ice. Proc. 3rd Intl Conf. on Permafrost, 10-13 July, Edmonton Alta., NRCC, Vol.1.

34. Josberger, E.G. 1977. A laboratory and field study of iceberg deterioration. Proceedings Iceberg Utilization, A.A.Husseiny (ed.), Pergamon Press, pp.245-264.

35. Kalske, S. 1993. A proposed nomenclature for coordinate systems in marine hydrodynamics. Ship Laboratory Report M-178, Helsinki University of Technology, 10 pp.

36. Ketchen, H.G. and Hildenbrand, R.N. 1977. Report of the International Ice Patrol Service in the North Atlantic, U.S. Coast Guard Bulletin No.63, CG-188-32, pp.D1-D2.

37. Kollmeyer, R.C. 1980. West Greenland outlet glaciers: an inventory of the major iceberg producers. Cold Regions Science and Technology, Vol.1, No.3 and 4, pp.175-181.

38. Kollmeyer, R.C. 1977. West Greenland glaciers: iceberg sources. Proceedings Iceberg Utilization, A.A.Husseiny (ed.), Pergamon Press, pp.25-28.

39. Kovacs, A. 1977. Iceberg thickness and crack detection. Proceedings Iceberg Utilization, A.A.Husseiny (ed.), Pergamon Press, pp.131-145.

40. Krimmel, R.M. and Vaughn, B.H. 1987. Columbia Glacier, Alaska: Changes in velocity 1977-1986. Journal of Geophysical Research, Vol.92, No.B9, pp.8961-8968.

41. Lee, R.W., and Schulson, E.M. 1986. The effect of grain size on the tensile strength of ice at two strain rates. Proc. OMAE, Vol.4, pp298-302.

42. Lever, J.H., Bass, D.W., Lewis, C.F.M., Klein, K., Diemand, D., and Dyke, M. 1991. Iceberg/seabed interaction events observed during the DIGS experiment. Journal of Offshore Mechanics and Arctic Engineering, ASME, Vol.113, pp.74-87.

43. Lewis, J.C. and Bennett, G. 1984. Monte Carlo calculations of iceberg draft changes caused by roll. Cold Regions Science and Technology, Vol.10, pp.1-10.

44. Løset, S. 1993. Thermal energy conservation in icebergs and tracking by temperature. Journal of Geophysical Research, Vol.98, No.C6, pp.10,001-10,012.

45. Martin, S., Josberger, E., and Kauffman, P. 1977. Wave-induced heat transfer to an iceberg. In Josberger, E.G. 1977. A laboratory and field study of iceberg deterioration. Proceedings Iceberg Utilization, A.A.Husseiny (ed.), Pergamon Press, pp.245-264.

46. McKenna, R.F., Crocker, G., and Paulin, M.J. 1999. Modelling iceberg scour processes on the northeast Grand Banks. Proceedings, Offshore Mechanics and Arctic Engineering, 10 pp.

47. Meier, M.F. and Post, A. 1987. Fast tidewater glaciers. Journal of Geophysical Research, Vol.92, No.B9, pp. 9051-9058.

48. Mountain, D.G. 1980. On predicting iceberg drift. Cold Regions Science and Technology, Vol.1, No.3 and 4, pp.273-282.

49. Paterson, W.S.B. 1994. The physics of glaciers, 3rd edition. Elsevier Science Ltd., Oxford, 480 pp.

50. Pelto, M.S. and Warren, C.R. 1991. Relationship between tidewater glacier calving velocity and water depth at the calving front. Annals of Glaciology, Vol.15, pp.115-118.

51. Pounder, E.R. 1965. Physics of ice. Pergamon Press, Oxford, 151 pp.

52. Reeh, N. 1968. On the calving of ice from floating glaciers and ice shelves. Journal of Glaciology, Vol.7, No.50, pp.215-232.

53. Riggs, N.P, Babu, P.V.T., Sullivan, M.A., and Russel, W.E. 1980. Iceberg drift observations in Lancaster Sound. Cold Regions Science and Technology, Vol.1, No.3 and 4, pp.283-291.

54. Robe, R.Q. 1980. Iceberg drift and deterioration. In Dynamics of snow and ice masses. Colbeck, S.C. (ed.). pp.211-260

55. Robe, R.Q., Maier, D.C., and Russel, W.E. 1980. Long-term drift of icebergs in Baffin Bay and the Labrador Sea. Cold Regions Science and Technology, Vol.1, No.3 and 4, pp.183-193.

56. Robe, R.Q., Maier, D.C., and Kollmeyer, R.C. 1977. Iceberg deterioration. Nature, Vol.267, pp.505-506.

57. Robe, R.Q., Maier, D.C., and Kollmeyer, R.C. 1976. Iceberg deterioration. Report of the International Ice Patrol Service in the North Atlantic, U.S. Coast Guard Bulletin No.62, CG-188-31, pp.60-64.

58. Russell, W.E., Riggs, N.P., and Robe, R.Q. 1977 (1978). Local iceberg motion - a comparison of field and model studies. Proc. POAC, St. John's, pp.784-798.

59. Russell-Head, D.S. 1980. The melting of free-drifting icebergs. Annals of Glaciology, Vol.1, pp.119-122.

60. Shirasawa, K., Riggs, N.P., and Muggeridge, D.B. 1984. The drift of a number of idealized model icebergs. Cold Regions Science and Technology, Vol.10, pp.19-30.

61. Sikonia, W.G. 1982. Finite element glacier dynamics model applied to Columbia Glacier, Alaska. Geological Survey Professional Paper 1258-B, 17 pp.74

62. Singh, S., Green, S., Ennis, T. Comfort, G., amd Davidson, L. 1998. PERD iceberg database for the Grand Banks region. Fleet Technology Ltd. for National Research Council, PERD/CHC Report 20-36, 29 pp. + app.

63. Smith, S.D. 1993. Hindcasting iceberg drift using current profiles and winds. Cold Regions Science and Technology, Vol.22, pp.33-45.

64. Smith, S.D. and Banke, E.G. 1983. The influence of winds, currents and towing forces on the drift of icebergs. Cold Regions Science and Technology, Vol.6, pp.241-255.

65. Smith, S.D. and Banke, E.G. 1981. A numerical model of iceberg drift. Proc. POAC, Vol.2, pp.1001-1012.

66. Sodhi, D.S. and El-Tahan, M. 1980. Prediction of an iceberg drift trajectory during a storm. Annals of Glaciology, Vol.1, pp.77-82.

67. Soulis, E.D. 1975. Modelling of drift of nearby icebergs using wind and current measurements at a fixed station. Canadian Society of Petroleum Geologists, pp.879-889.

68. Venkatesh, S., El-Tahan, M., and Mitten, P.T. 1985. An Arctic iceberg deterioration field study and model simulations. Annals of Glaciology, Vol.6, pp. 195-199.

69. Venkatesh, S. 1986. On the deterioration of a grounded iceberg. Journal of Glaciology, Vol.32, No.111, pp.161-167.

70. Venkatesh, S. and El-Tahan, M. 1988. Iceberg life expectancies in the Grand Banks and Labrador Sea. Cold Regions Science and Technology, Vol.15, pp.1-11.

71. Venkatesh, S., Murphy, D.L., and Wright, G.F. 1994. On the deterioration of icebergs in the marginal ice zone. Atmosphere-Ocean, Vol.32, No.2, pp.469-484.

72. Weeks, W.F. and Mellor, M. 1977. Some elements of iceberg technology. Proceedings Iceberg Utilization, A.A.Husseiny (ed.), Pergamon Press, pp.45-98.

73. Weidick, A., Bøggild, C.E., and Knudsen, N.T. 1992. Glacier inventory and atlas of West Greenland. Grønlands Geologiske Undersøgelse Rapport 158, 194 pp.

74. White, F.M., Spaulding, M.L., and Gominho, L. 1980. Theoretical estimates of the various mechanisms involved in iceberg deterioration in the open ocean environment. University of Rhode Island for United States Coast Guard, CG-D-62-80, 126 pp.

Annex A - Ice Block Melting Tests

Introduction

A set if ice block melting tests were carried out by K. Daley [14]. This Annex summarizes the results of those tests. Blocks of ice, representing icebergs, were used to study how icebergs melt and what factors affect the melting. The blocks were tested in three different conditions, and 10 tests were performed. All tests were conducted in a small tank, with a depth of 34 cm and water temperature of from 15°C to 16°C. The air temperature was about 17.5°C. Two different block sizes were used. The first was a cube, (0.248m x 0.248m x 0.254m), and the second was a slab (0.273m x 0.197m x 0.152m).

Photo A1. Block No. 1, soon after start.

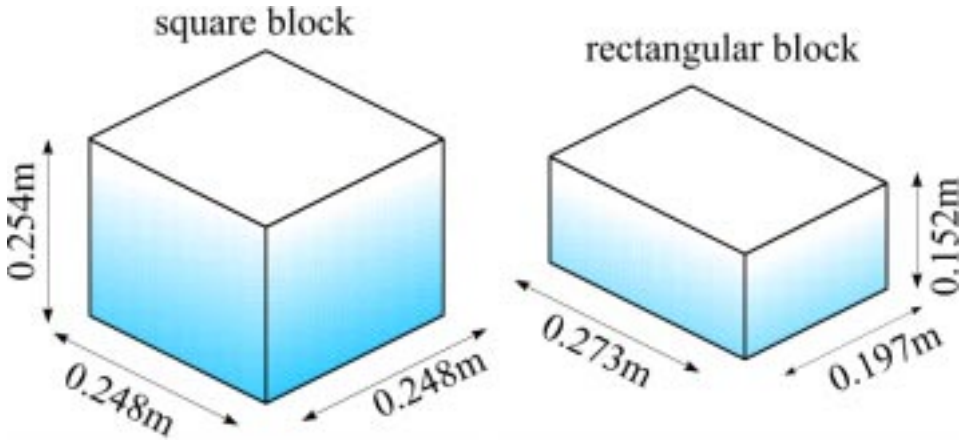

Figure A1. Block dimensions.

The test conditions were as follows:

- Condition 1 - calm water, tests 1 to 4.
- Condition 2 - small waves (1-2 mm, 3 Hz), tests 5 to 8.
- Condition 3 - calm water + 100W lamp, tests 9 and 10.

Table 1 shows all the actual test conditions.

Table A7. Test Parameters

Test #	Block Shape	Volume [$10^{-3}m^3$]	Weight [kg]	Water temp. [°C]	Block temp. [°C]	Air temp. [°C]	Waves [yes/no]	Lamp [yes/no]
1	cube	15.62	13.61	15	-25	17.5	no	no
2	cube	15.62	13.83	15	-31.3	17	no	no
3	slab	8.174	7.335	15.5	-31.9	17	no	no
4	slab	8.174	6.971	16	-31.1	17	no	no
5	cube	15.62	14.402	15.5	-31.2	18	yes	no
6	cube	15.62	13.787	16	-25	19	yes	no
7	slab	8.174	7.34	16	-30.8	18	yes	no
8	slab	8.174	7.383	16	-31.4	18.5	yes	no
9	cube	15.62	13.698	16	-31.4	18.5	no	yes
10	cube	15.62	14.288	16	-31.4	18.5	no	yes

Table A8. Results summary

Test #	# of Rolls	Time to Melt [min]
1	7	127
2	7	105 *
3	6	87
4	5	82
5	19	102
6	15	102
7	11	77
8	6	77
9	5	114
10	8	110

*this data point seems wrong.

Figures A2 to A6 show the mass and roll event vs time. Each plot shows that two tests for the same conditions. In all cases the rate of mass loss was highest at the start, while the rate of rolling increased with time.

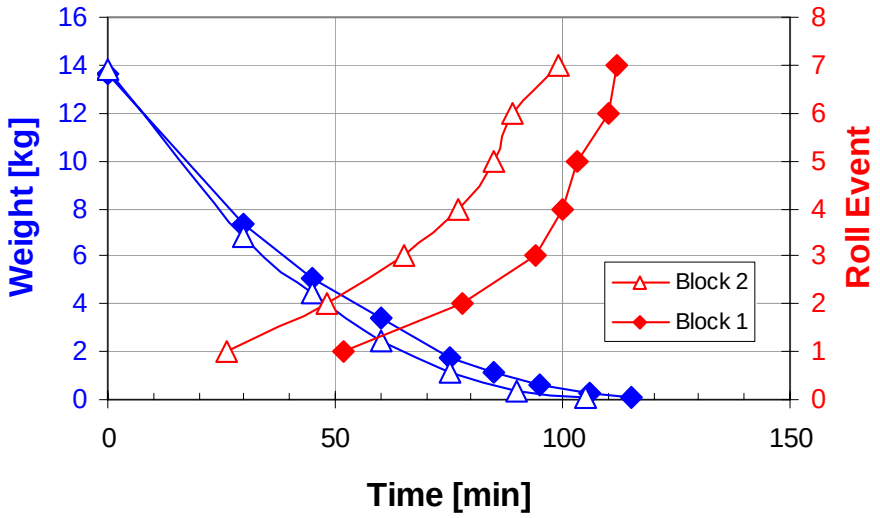

Figure A2. Weight-time and Roll-time comparisons for Blocks 1 & 2.

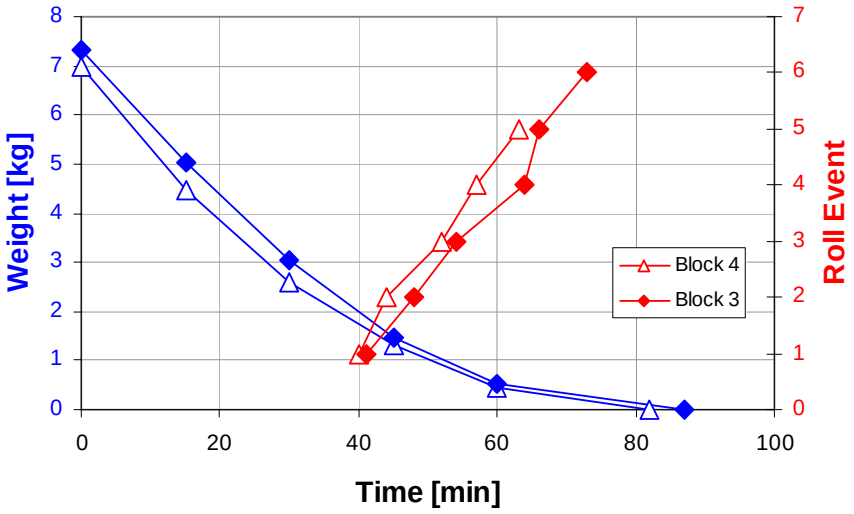

Figure A3.Weight-time and Roll-time comparisons for Blocks 3 & 4.

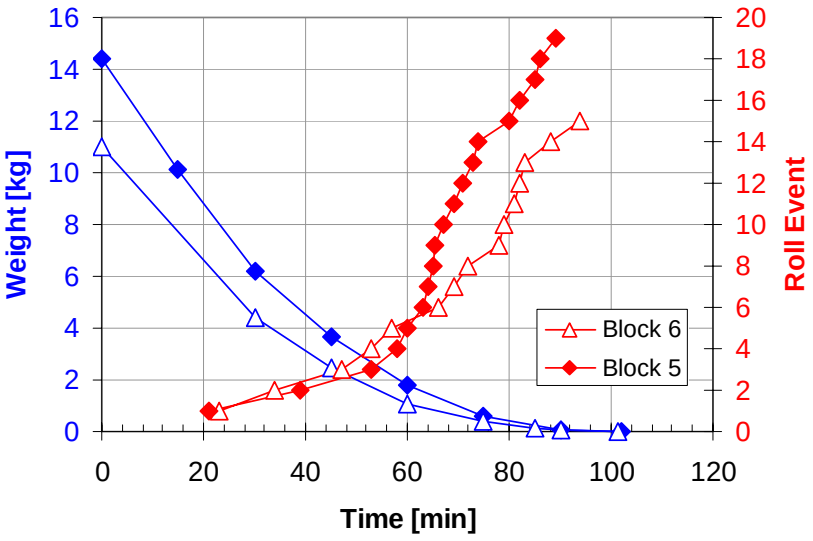

Figure A4. Weight-time and Roll-time comparisons for Blocks 5 & 6.

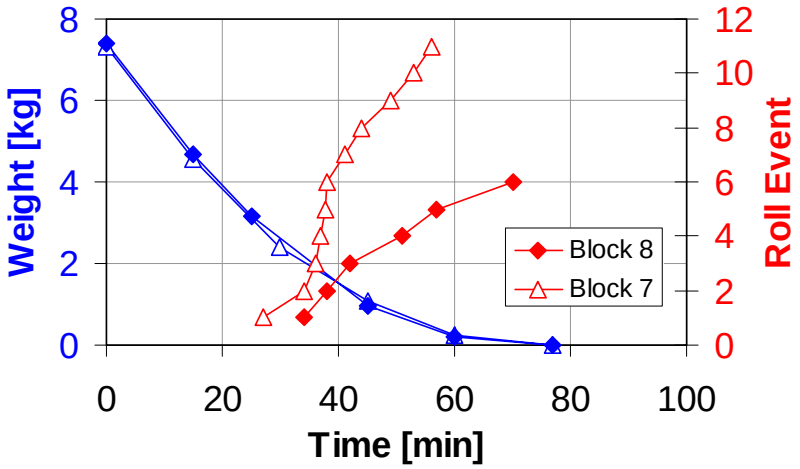

Figure A5. Weight-time and Roll-time comparisons for Blocks 7 & 8.

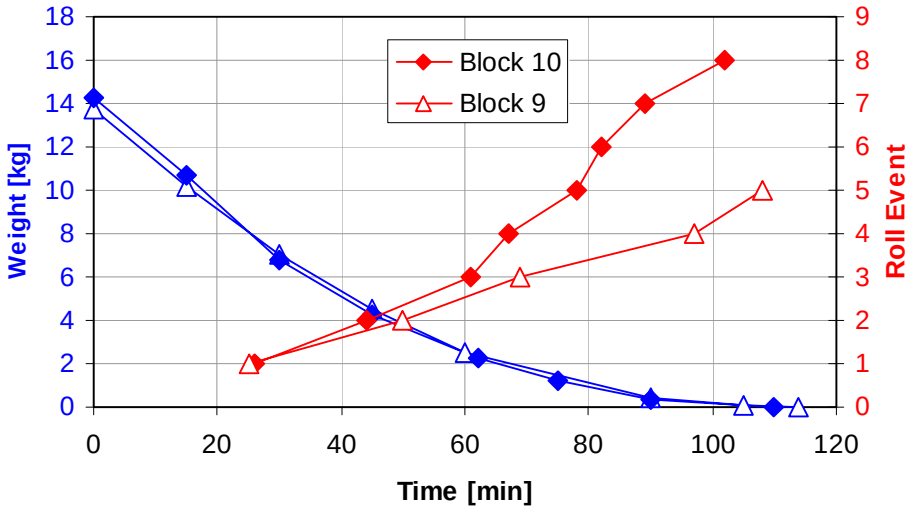

Figure A6. Weight-time and Roll-time comparisons for Blocks 9 & 10.

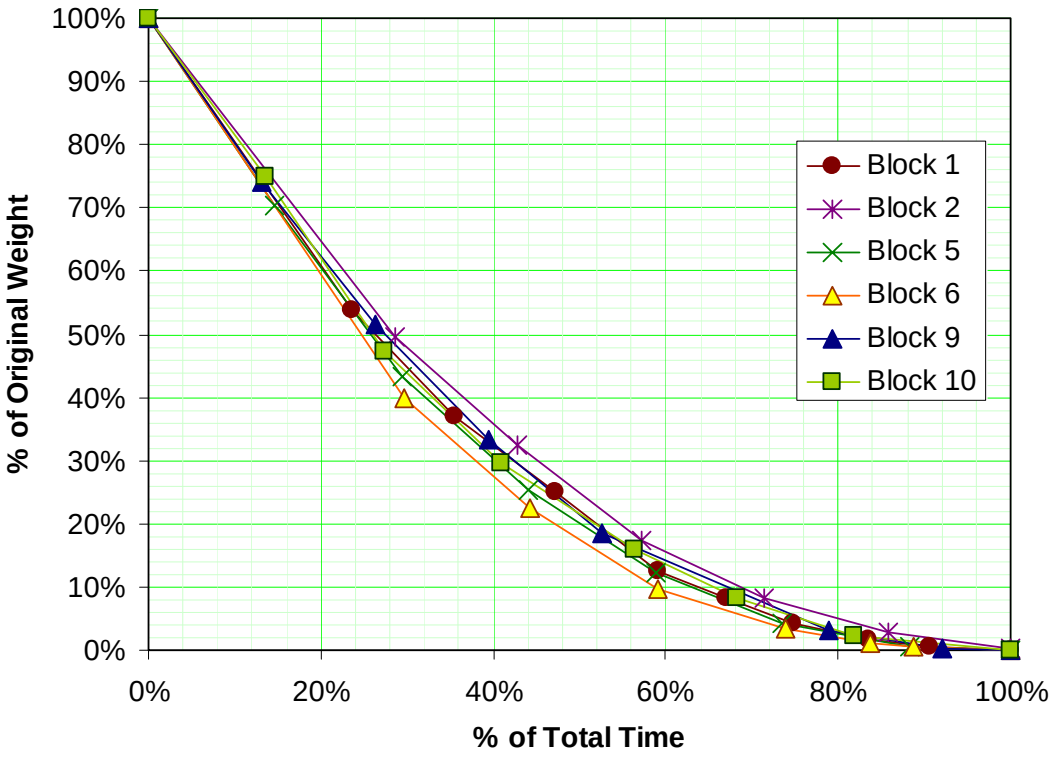

Figure A7. Percent Weight-Time Graphs for Square Blocks

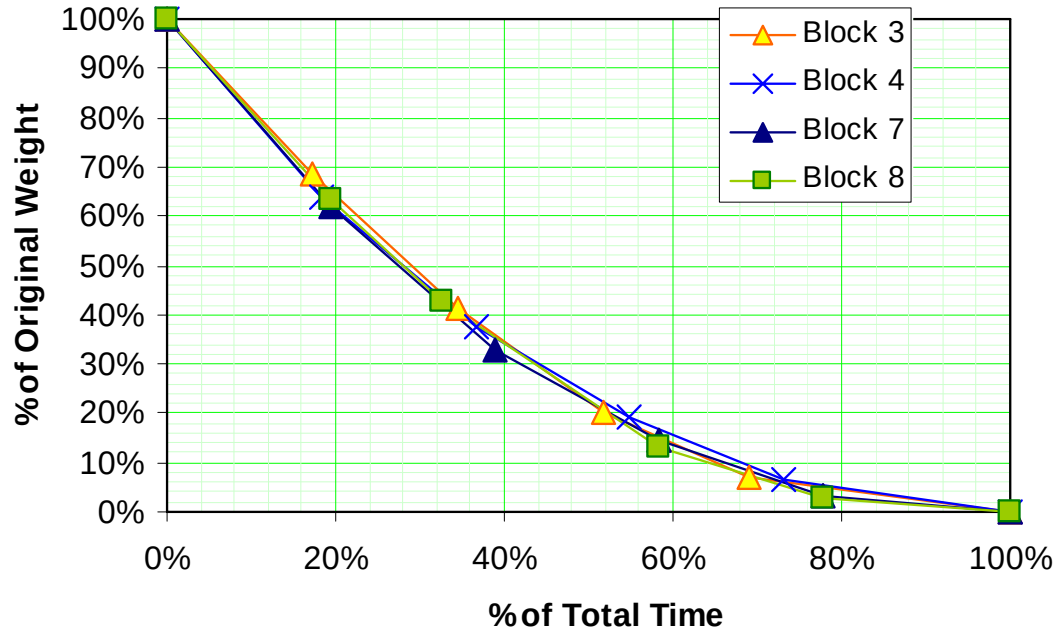

Figure A8. Percent Weight-Time Graphs for Rectangular Blocks

All tests were performed twice. Generally, both blocks of a given condition behaved in a similar manner. For most of the test pairs, the number of rolls varied significantly between blocks (see Figures A4, A5, A6). Rolling seems to be more unpredictable than melting. As rolling occurs due to instability and melting is a stable process, it is not surprising that rolling is less predictable.

All blocks melted faster in the first part of the tests. This is because the surface area reduced as the block melted, so the rate of mass loss was reduced. In Figures A7 and A8, above, it is shown that all of the blocks (square and rectangular) in all of the tests showed a similar pattern of melt (i.e. % mass vs %time). The melting analysis, following this section, presents models of different theoretical melting scenarios and equations to explain them.

The condition that had the most effect on the melting, in comparison to the calm water tests, were waves (tests 5 to 8). As seen in Table 2 and in Figures A4 and A5, the waves caused the blocks to melt faster, though not by a large amount. The biggest difference was that the waves caused a sharp increase in the number of rolls, and the blocks started to roll earlier. Because the rolls started earlier, the blocks usually became more rounded, therefore more unstable, and that in turn caused more rolls. Despite this increase in rolling and faster melting, the waves did not seem to make a difference on the % mass vs. % percent time graphs (Figs. A7 and A8). This is an interesting observation. This suggests that while waves or radiation may speed the melting, they do not seem to affect the mass/time pattern of melting. The lamp seemed to have little effect on the melting (tests 9 and 10), though the melting times were less than in tests without the lamp.

The shape of the block did affect the behavior of the ice. The square blocks and the rectangular blocks each had their different melting/rolling patterns. The square block would melt, forming a "lip" at the surface, until it became unstable, then roll 90° (See Photo A2). It would become relatively stable after the roll, until one side melted a little more than the other, and then would roll again. This pattern would repeat itself (especially for tests 1 and 2) throughout the whole test, except near the very end. However, a rectangular prism is naturally a more stable shape than a cube. While a cube can easily roll to any side, a rectangle will roll only

to its sides, not its ends. This is exactly what happened during the tests. The rectangular blocks were later to roll, and generally less throughout the tests. As well, the rolls were not usually 90°, as for the cubic blocks, but about 45°. This rolling pattern produced something similar to a trapezoid, which is also a stable shape. Nevertheless, as previously stated, these differences in the tests did not seem to affect the % mass-% time graph (Fig. 9).

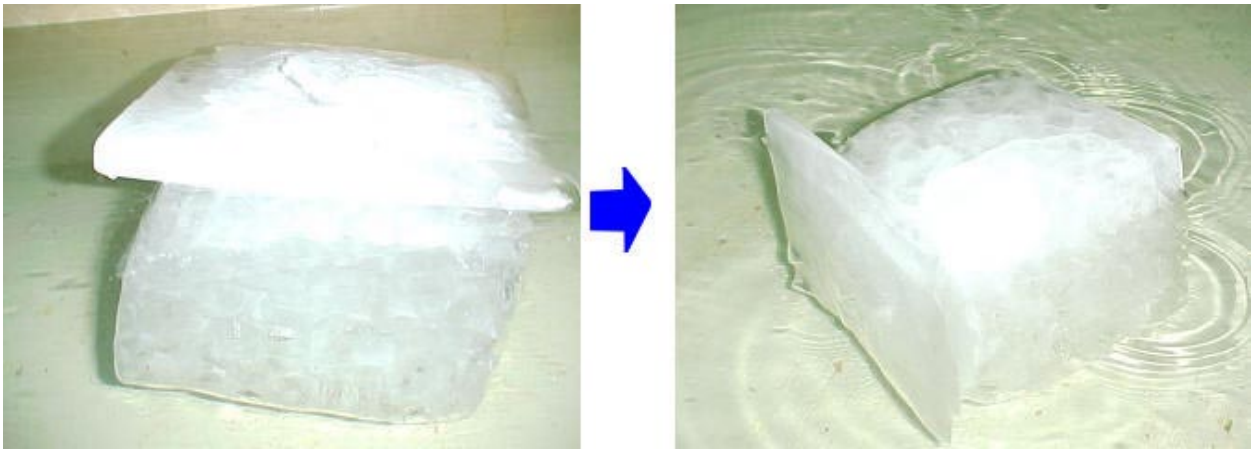

Photo A2. Typical 90° roll event for cubic ice blocks.

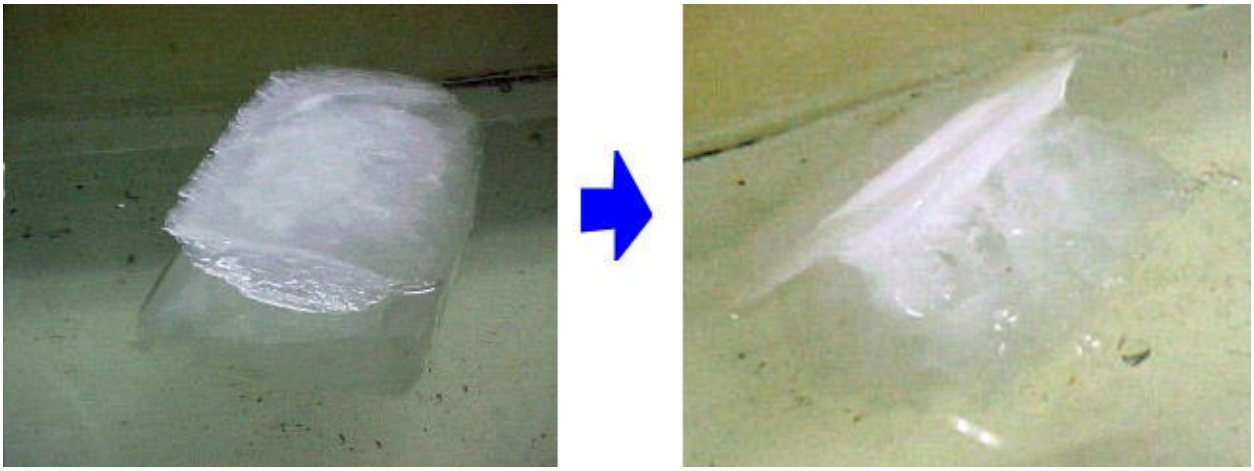

Photo A3. Typical ~45° roll event for rectangular ice blocks.

Melting Analysis

White et. al.[74], reported on a similar experiment (ice block melting). An equation was given to describe the melting rate of a block melting in waves (with very similar conditions);

$$m/m_s = (1-t/t_f)\,(1-0.36\,t/t_f) \qquad \text{(W81)}$$

As shown in Figure A9, equation W81 was not close to the data collected in these tests (nor was it close to White's data). A new equation has been derived to attempt to better explain the melting of the blocks.

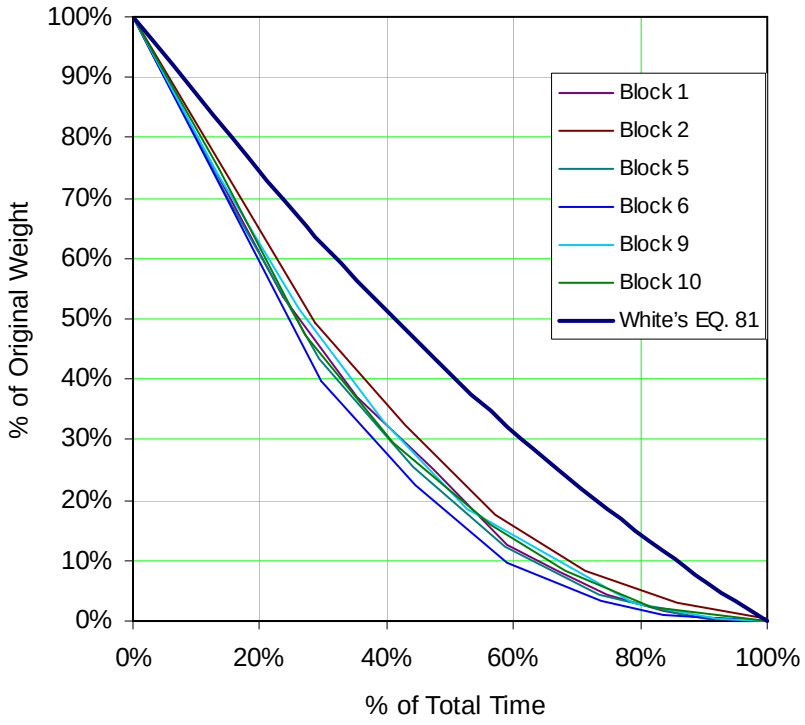

Figure A9. Measured block data compared to White et.al. EQ 81.

In order to derive a melting equation, a pattern of melting must be assumed. Four cases for how an ice block can melt are described. In Case 1 (Figure A10) the ice block is completely submerged, and melting from all sides, top and bottom. In Case 2 (Figure A11), the ice is

melting from the sides only and not the top or bottom. In Case 3 (Figure A12) the ice block is floating just at the surface, so that the 4 sides and the bottom are melting, but not the very top. In Case 4 (Figure A13), which is the closest to the experiments performed, part of the sides and bottom are melting. With 7/8 of the sides under water, a simple assumption is made that the whole side melts at 7/8 the rate of the bottom. Therefore, Case 4 is a small variation on Case 3. The equations below were derived to help explain the melting process.

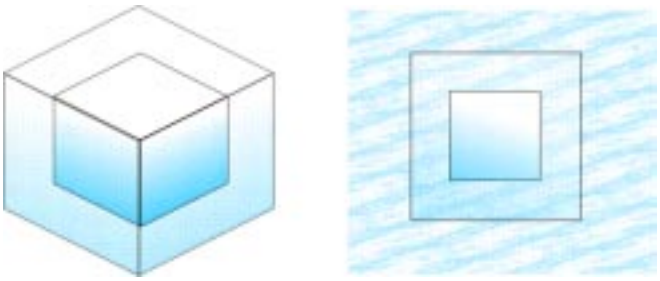

Figure A10. Case 1 melting assumption.

Case 1

In this case, all 4 sides, top and bottom are underwater and melting at the same rate. All dimensions are equal and given as *W*. *W* reduces from its initial value to zero, evenly in time. An equation for *W* must be linear and of the form;

$$W = mt + b \qquad \text{(A1)}$$

where W is the width, m is the slope, t is the time, and b is the x-intercept. The slope is $m = -W_s/tf$, and $b = W_s$, where W_s is the width at the start, and t_f is the time when the block has completely melted. From this,

$$W = -W_s*t/t_f + W_s \qquad \text{(A2)}$$

$$W = W_s(1-t/t_f) \qquad \text{(A3)}$$

The mass at the start (m_s), is equal to the volume ($W_s*D_s*H_s$) multiplied by the density of ice (ρ_{ice}). Because the ice block is a cube, $W_s = D_s = H_s$, therefore,

$$m_s = W_s^3 * \rho_{ice} \qquad \text{(A4)}$$

An equation can be written from this for any mass, *m*;

$$\begin{aligned} m &= W*D*H*\rho_{ice} \\ &= W^3 \rho_{ice} \\ &= W_s^3(1-t/t_f)^3 \rho_{ice} \end{aligned} \quad \text{(A5)}$$

An equation for the ratio of mass of the block to the mass at the start is;

$$\begin{aligned} m/m_s &= [W_s^3(1-t/t_f)^3 * \rho_{ice}]/[W_s^3 * \rho_{ice}] \\ &= (1-t/t_f)^3 \end{aligned} \quad \text{(A6)}$$

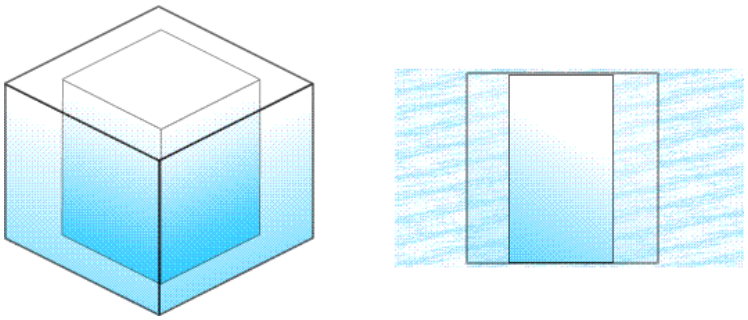

Figure A11. Case 2 melting assumption.

Case 2

In this case, only the 4 sides are melting. Equations (A1) through (A4) remain the same. For this case equation (A5) becomes;

$$\begin{aligned} m &= D*W*H_s*\rho_{ice} \\ &= W^2 * W_s \rho_{ice} \\ &= W_s^3(1-t/t_f)^2 \rho_{ice} \end{aligned} \quad \text{(A7)}$$

Therefore the equation for the ratio of the mass of the block to the mass at the start is;

$$\begin{aligned} m/m_s &= [W_s^3(1-t/t_f)^2 * \rho_{ice}]/[W_s^3 * \rho_{ice}] \\ &= (1-t/t_f)^2 \end{aligned} \quad \text{(A8)}$$

[Note: this equation is identical to EQ 80 in White et.al. [74]]

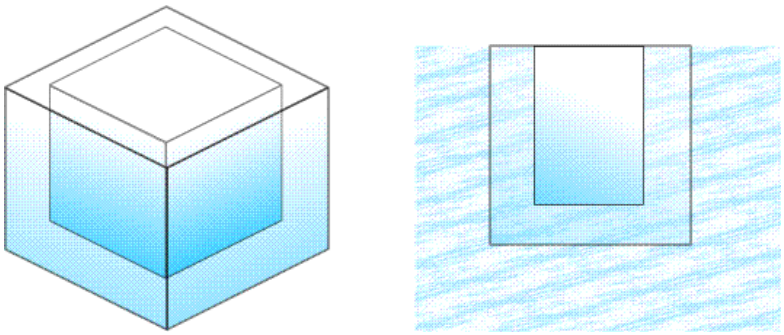

Figure A12. Case 3 melting assumption.

Case 3

In this case, the 4 sides and the bottom are melting. Equations (A1) through (A4) remain the same. The height of the block reduces at 1/2 the speed that the width is reducing. In other words, when the width reduces to zero, the height has reduced to $W_s/2$. The equation describing the height in time is;

$$H = W_s\,(1\text{-}t/2t_f\,) \qquad \text{(A9)}$$

For this case equation (A5) becomes;

$$\begin{aligned} m &= W{*}D{*}H{*}\,\rho_{ice} \\ &= W^2\,W_s\,(1\text{-}t/2t_f\,)\,\rho_{ice} \\ &= W_s^3(1\text{-}t/t_f)^2(1\text{-}t/2t_f)\,\rho_{ice} \end{aligned} \qquad \text{(A10)}$$

Therefore the equation for the ratio of the mass of the block to the mass at the start is;

$$\begin{aligned} m/m_s &= [W_s^3(1\text{-}t/t_f)^2{*}(1\text{-}t/2t_f)\,\rho_{ice}]/[W_s^3{*}\,\rho_{ice}] \\ &= (1\text{-}t/t_f)^2{*}(1\text{-}t/2t_f) \end{aligned} \qquad \text{(A11)}$$

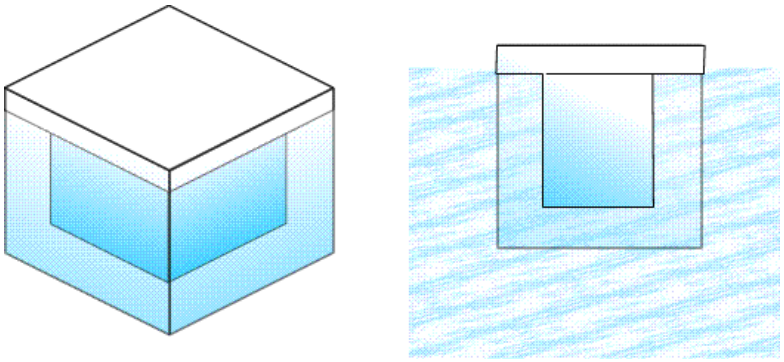

Figure A13. Case 4 melting assumption.

Case 4

In this case, the 4 sides are only partly (7/8^{ths}) submerged. To model this in a simple way, it is assumed that the sides are melting at 7/8ths the rate of the bottom. However, as the block disappears when the width becomes zero, it is better to say that the bottom is melting at 8/7ths as fast as the sides (remember: all times and sizes are relative). Equations (A1) through (A4) remain the same. The height of the block reduces at 4/7ths (8/7 x 1/2 =) the speed that the width is reducing. In other words, when the width reduces to zero, the height has reduced to 3/7 W_s. The equation describing the height in time is;

$$H = W_s\,(1\text{-}4/7\ t/t_f\,) \qquad \text{(A12)}$$

For this case equation (A5) becomes;

$$\begin{aligned} m &= W*D*H*\rho_{ice} \\ &= W^2\ W_s\,(1\text{-}4/7\ t/t_f\,)\ \rho_{ice} \\ &= W_s^3(1\text{-}t/t_f)^2(1\text{-}4/7\ t/t_f)\ \rho_{ice} \end{aligned} \qquad \text{(A13)}$$

Therefore the equation for the ratio of the mass of the block to the mass at the start is;

$$\begin{aligned} m/m_s &= [W_s^3(1\text{-}t/t_f)^2*(1\text{-}4/7\ t/t_f)\ \rho_{ice}]/[W_s^3*\rho_{ice}] \\ &= (1\text{-}t/t_f)^2*(1\text{-}4/7t/t_f) \end{aligned} \qquad \text{(A14)}$$

Figure 14 shows the measured data and equations (A6,A8,A11,A14). It is clear that equations (A11) and (A14) are better that the simpler equations (A6, A8).

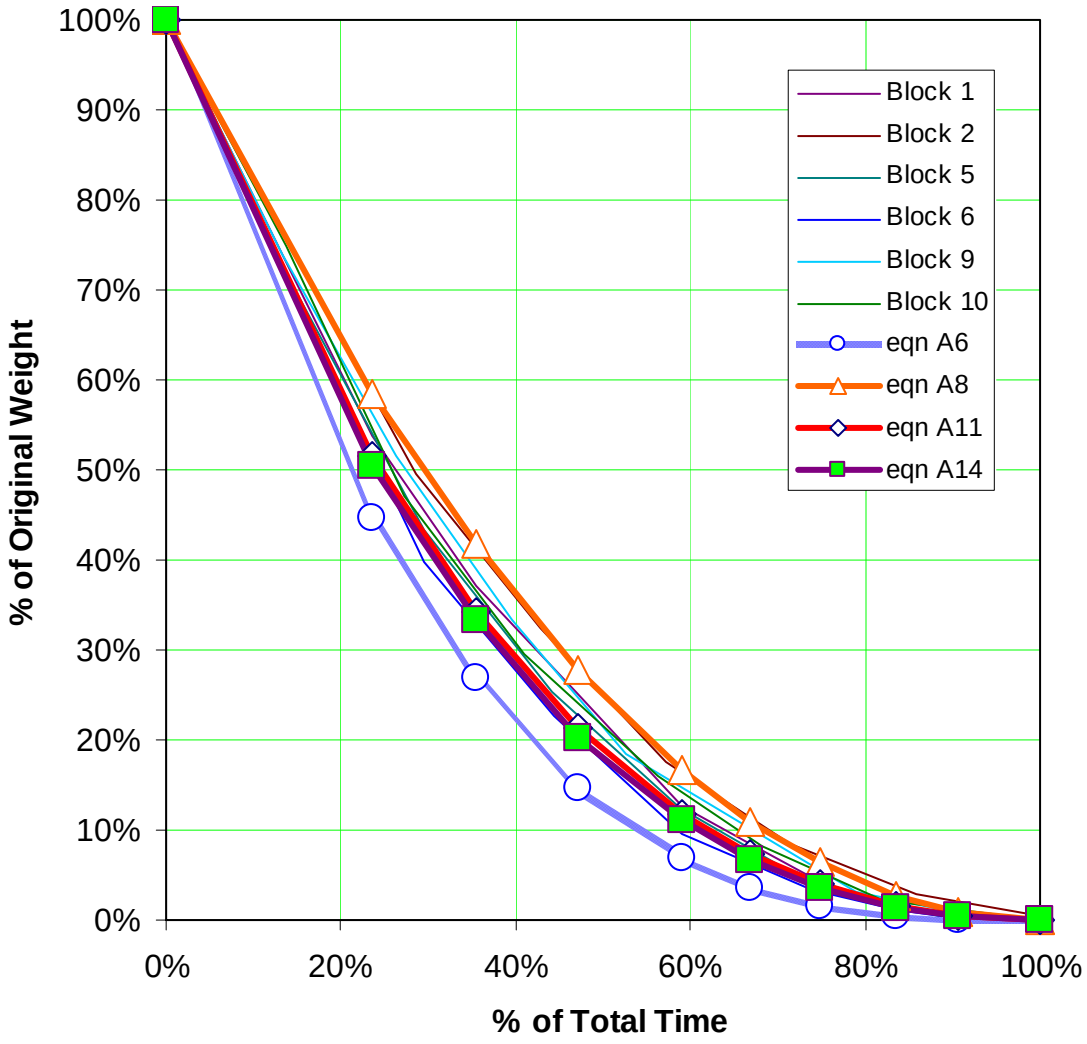

Figure A14. Measured data compared to equations.